

# Search for a light $Z'$ at LHC in a neutrinophilic $U(1)$ model

Waleed Abdallah,<sup>1,2,\*</sup> Anjan Kumar Barik,<sup>1,†</sup> Santosh Kumar Rai,<sup>1,‡</sup> and Tousik Samui<sup>1,§</sup>

<sup>1</sup>*Regional Centre for Accelerator-based Particle Physics,*

*Harish-Chandra Research Institute, HBNI,*

*Chhatnag Road, Jhansi, Prayagraj (Allahabad) 211 019, India*

<sup>2</sup>*Department of Mathematics, Faculty of Science,*

*Cairo University, Giza 12613, Egypt*

## Abstract

We consider a neutrinophilic  $U(1)$  extension of the standard model (SM) which couples only to SM isosinglet neutral fermions, charged under the new group. The neutral fermions couple to the SM matter fields through Yukawa interactions. The neutrinos in the model get their masses from a standard inverse-seesaw mechanism while an added scalar sector is responsible for the breaking of the gauged  $U(1)$  leading to a light neutral gauge boson ( $Z'$ ) which has minimal interaction with the SM sector. We study the phenomenology of having such a light  $Z'$  in the context of neutrinophilic interactions as well as the role of allowing kinetic mixing between the new  $U(1)$  group with the SM hypercharge group. We show that current experimental searches allow for a very light  $Z'$  if it does not couple to SM fields directly and highlight the search strategies at the LHC. We observe that multi-lepton final states in the form of  $(4\ell + \cancel{E}_T)$  and  $(3\ell + 2j + \cancel{E}_T)$  could be crucial in discovering such a neutrinophilic gauge boson lying in a mass range of 200–500 GeV.

---

\* [awaleed@sci.cu.edu.eg](mailto:awaleed@sci.cu.edu.eg)

† [anjanbarik@hri.res.in](mailto:anjanbarik@hri.res.in)

‡ [skrai@hri.res.in](mailto:skrai@hri.res.in)

§ [tousiksamui@hri.res.in](mailto:tousiksamui@hri.res.in)

## I. INTRODUCTION

The modern era of particle physics has seen an extremely successful period with the model accounting for three of fundamental interactions of nature via gauge symmetries, i.e. the standard model (SM) of particle physics. The SM successfully explains most phenomena involving the elementary particles in nature which have been corroborated through observations in dedicated experiments. The discovery of a 125 GeV scalar [1, 2] *viz.* the Higgs boson has completed the hunt for all particles predicted in the SM. Despite the remarkable success of the SM, there still remain several unexplained observations from experiments that hint at the possibility of new physics beyond the SM (BSM). One such anomaly is the observation of non-zero mass and mixing of neutrinos from neutrino oscillation experiments [3–7]. The otherwise massless neutral fermion within the SM can, in competing BSM extensions, have either Dirac or Majorana type mass which is something yet to be established. A large number of scenarios exist to explain observed neutrino masses and mixings [8–12] and these possibilities lead to interesting phenomenology of the resulting neutrino mass models [13]. Besides the neutrino mass puzzle, another curiosity which intrigues us is the true nature of the scalar that has been observed at the Large Hadron Collider (LHC). The complete confirmation of it being the SM Higgs will only be possible, once its interactions are precisely measured. Until then it does leave the possibility of new physics within the scalar sector as a vital area of interest. There are a vast number of BSM theories including some for neutrino mass models, which include an extended scalar sector beyond the SM Higgs doublet. Our focus would be on the type which is central to neutrino mass models.

The minimal extension of the scalar sector is usually done with or without a new gauge group, although an extended scalar sector is more natural in extended gauge models where the scalars are charged under the new gauge group and are responsible for the spontaneous breaking of the new gauge symmetry. All such extensions predict some new phenomena which is to be observed in ongoing and upcoming experiments. Extension of the SM with an additional Higgs doublet is one of the most popular extension of the SM and popularly known as the two Higgs doublet models (2HDM). In some models the second Higgs doublet is used to give Dirac masses to the light neutrinos by introducing new right-handed neutrinos. Such models are popularly called neutrinophilic 2HDM ( $\nu$ 2HDM) [14–16], which lead to interesting phenomenology and signatures at experiments [17–22]. Another popular

extension of the SM is the extension with a new  $U(1)$  gauge group. The introduction of new gauge groups have a different type of consequence, in terms of signature of the model. One immediate consequence is the prediction of a new massive gauge boson ( $Z'$ ) after the symmetry breaking of the new  $U(1)$  symmetry. The work in this article incorporates both these types of extensions into a single framework.

We consider an extra  $U(1)$  symmetry under which the SM particles are sterile. This is more in the line of a hidden extra  $U(1)$  considered before in another context by one of us [23, 24]. Only new SM isosinglet fermions, an electroweak (EW) singlet scalar and a neutrinophilic Higgs doublet speak to this extra  $U(1)$ . These new fields act as messenger particles between the  $U(1)$  and the SM sector. The extra  $U(1)$  symmetry is broken at the EW scale by the vacuum expectation value (VEV) of an EW singlet Higgs boson along with the second Higgs doublet. Thus the model predicts a heavy  $Z'$  at the EW scale along with additional neutral fermions and scalar particles. We show through this work that the prediction of such an extension of the SM which can explain the light neutrino mass and with a particle spectrum which has minimal interactions to the charged fermions has its own set of challenges of observation and how such a scenario can be observed in the ongoing collider experiments.

The search for  $Z'$  boson has been extensively studied at the LHC where most of the searches put strong limits on the mass of the  $Z'$  based on its interaction properties [25, 26]. The most popular channel to search for  $Z'$  is usually the dilepton channel which gives stringent constraint on the production of  $Z'$  at the LHC [27, 28]. However, in our model, an interesting scenario arises where the  $Z'$  can be significantly lighter than current limits and can evade bounds from the existing  $Z'$  search. For such a  $Z'$  we find that the multi-lepton channel proves much more promising. In this study, we mainly focus on  $Z'$  from the viewpoint of its neutrinophilic nature.

The paper is organised as follows. In section II we briefly discuss the framework of the  $U(1)$  gauged neutrinophilic model and calculate the mass and mixing parameters for the scalar, gauge and fermion sectors in the model. In section III we discuss the relevant theoretical and experimental constraints before we move on to section IV where we present the LHC analysis of the model in the  $4\ell$  and  $3\ell$  rich final states coming from the  $Z'$  mediated heavy neutrino production. Finally we summarise and conclude in section V.

## II. THE MODEL

The model is an extension of the SM where the gauge group is augmented with an extra  $U(1)_X$  gauge group and four new fields, *viz.* a second Higgs doublet ( $H_2$ ), a scalar singlet ( $S$ ), and two chiral sterile neutrinos ( $N_L, N_R$ ) added for each generation. All the new fields are charged under the gauge group  $U(1)_X$  while all the SM particles are neutral. The charge assignments of the new particles along with the first Higgs doublet ( $H_1$ ), which is the SM Higgs doublet, are listed in Table I. Looking at the charge assignments, it is quite clear why

Fields	$SU(3)_C$	$SU(2)_L$	$U(1)_Y$	$U(1)_X$	Spin
$H_1$	1	2	$-1/2$	0	0
$H_2$	1	2	$-1/2$	$-q_x$	0
$S$	1	1	0	$2q_x$	0
$N_L^i$	1	1	0	$q_x$	1/2
$N_R^i$	1	1	0	$q_x$	1/2

TABLE I. New scalar ( $H_a, S$ , a=1,2) and matter ( $N_L^i, N_R^i$ , i=1,2,3) fields and their charge assignments under the SM gauge group and  $U(1)_X$ .

we refer the model as a neutrinophilic one. The new isosinglet charge-neutral fermions are the only spin-1/2 fields which carry a  $U(1)_X$  charge and therefore would lead to couplings of the new gauge boson with the neutrinos after symmetry breaking.

With the assigned charges, the most general gauge invariant Lagrangian that can be added to the SM Lagrangian, is given by

$$\begin{aligned}
\mathcal{L} \supset & (D_\mu H_1)^\dagger D_\mu H_1 + (D_\mu H_2)^\dagger D_\mu H_2 + (D_\mu S)^\dagger D_\mu S - \mu_1 H_1^\dagger H_1 - \mu_2 H_2^\dagger H_2 - \mu_s S^\dagger S \\
& + i \bar{N}_L \gamma^\mu D_\mu N_L + i \bar{N}_R \gamma^\mu D_\mu N_R - \hat{M}_N (\bar{N}_L N_R + \bar{N}_R N_L) - \{Y_\nu \bar{l}_L H_2 N_R + h.c.\} \\
& - \lambda_1 (H_1^\dagger H_1)^2 - \lambda_2 (H_2^\dagger H_2)^2 - \lambda_{12} H_1^\dagger H_1 H_2^\dagger H_2 - \lambda'_{12} |H_1^\dagger H_2|^2 \\
& - \lambda_s (S^\dagger S)^2 - \lambda_{1s} H_1^\dagger H_1 S^\dagger S - \lambda_{2s} H_2^\dagger H_2 S^\dagger S - \{Y_R S \bar{N}_R N_R^C + Y_L S \bar{N}_L N_L^C + h.c.\} \\
& + \left\{ \mu_{12} H_1^\dagger H_2 + h.c. \right\} .
\end{aligned} \tag{1}$$

Note that the last term in the Lagrangian breaks the  $U(1)_X$  symmetry explicitly. This soft-breaking term is needed to give mass to the pseudo-scalar after the symmetry breaking.

In addition, the singlet scalar  $S$  plays a crucial role in defining the mechanism for neutrino mass generation, notwithstanding the fact that it is also responsible for the mass of the  $U(1)_X$  gauge boson. We shall now discuss the mass and mixings of the scalars, gauge bosons and matter fields following the spontaneous symmetry breaking (SSB) of the gauge symmetries.

### A. Masses and mixing of the scalars

The  $U(1)_X$  symmetry is spontaneously broken when either the singlet  $S$  or the doublet  $H_2$  acquires a VEV while the SM gauge symmetry breaks when either of the two Higgs doublets get a VEV. The Higgs doublets and the scalar singlet fields can be redefined by shifting with their VEVs in the usual way. Defining the VEVs for the Higgs doublets and singlet  $S$  as  $v_1$ ,  $v_2$ , and  $v_s$ , respectively, we can rewrite the fields as follows:

$$H_1 = \begin{pmatrix} \frac{v_1 + \rho_1 + i\eta_1}{\sqrt{2}} \\ \phi_1^- \end{pmatrix}, \quad H_2 = \begin{pmatrix} \frac{v_2 + \rho_2 + i\eta_2}{\sqrt{2}} \\ \phi_2^- \end{pmatrix}, \quad S = \frac{v_s + \rho_s + i\eta_s}{\sqrt{2}}. \quad (2)$$

In order for the potential to be minimum at the values of the VEVs, they should satisfy the following tadpole equations.

$$\mu_1 - \mu_{12} \frac{v_2}{v_1} + \lambda_1 v_1^2 + \frac{\lambda_{12} + \lambda'_{12}}{2} v_2^2 + \frac{\lambda_{1s}}{2} v_s^2 = 0, \quad (3)$$

$$\mu_2 - \mu_{12} \frac{v_1}{v_2} + \lambda_2 v_2^2 + \frac{\lambda_{12} + \lambda'_{12}}{2} v_1^2 + \frac{\lambda_{2s}}{2} v_s^2 = 0, \quad (4)$$

$$\mu_s + \frac{\lambda_{1s}}{2} v_1^2 + \frac{\lambda_{2s}}{2} v_2^2 + \lambda_s v_s^2 = 0. \quad (5)$$

After the spontaneous breaking of the EW and  $U(1)_X$  symmetries, we are left with three physical CP even neutral Higgses, a charged Higgs and a pseudo-scalar Higgs. Following the restrictions given by the above minimization conditions, the mass matrix for the pseudo-scalars in  $(\eta_1 \ \eta_2 \ \eta_s)^T$  basis becomes

$$M_A^2 = \frac{\mu_{12}}{v_1 v_2} \begin{pmatrix} v_2^2 & -v_1 v_2 & 0 \\ -v_1 v_2 & v_1^2 & 0 \\ 0 & 0 & 0 \end{pmatrix}. \quad (6)$$

It is evident from the mass matrix that two pseudo-scalars remain massless after the diagonalization to their mass eigenstates. These two massless modes are eaten up by the two

neutral gauge bosons, *viz.*  $Z$  and  $Z'$ , to acquire masses. The remaining pseudo-scalar is a physical state with a mass  $m_A = \sqrt{\frac{\mu_{12}}{v_1 v_2}} v^2$ , where  $v = \sqrt{v_1^2 + v_2^2} \simeq 246$  GeV.

It is worth noting that if the soft-breaking term was absent, i.e.  $\mu_{12} = 0$  in the Lagrangian given in Eq. (1), all the pseudo-scalars would have been massless. This is expected since, in the scalar sector of the Lagrangian, one can recover a global  $U(1)$  symmetry, *viz.*  $\phi \rightarrow e^{-i\theta Q} \phi$ , where  $\phi$  represents any of the scalars. This global symmetry remains intact even after both the SM and  $U(1)_X$  gauge symmetries are spontaneously broken, leading to a massless physical scalar in the particle spectrum. The soft-breaking term is therefore needed to avoid this massless pseudo-scalar.

The mass matrix of the charged scalars in  $(\phi_1^+ \ \phi_2^+)^T$  basis is given by

$$M_{\pm}^2 = \left( \frac{\mu_{12}}{v_1 v_2} - \frac{\lambda'_{12}}{2} \right) \begin{pmatrix} v_2^2 & -v_1 v_2 \\ -v_1 v_2 & v_1^2 \end{pmatrix}. \quad (7)$$

This  $2 \times 2$  mass matrix can be easily diagonalised by rotating with an angle  $\beta$  which is defined by the ratio of the VEVs of the two Higgs doublets given by  $\tan \beta = \frac{v_2}{v_1}$ . It should be noted that the same angle  $\beta$  also diagonalises the pseudo-scalar mass matrix. One of the charged scalar is massless and corresponds to the charged Goldstone which is eaten up by  $W^{\pm}$  gauge boson to get its mass. The remaining physical charged scalar is orthogonal to the massless one and is given by

$$H^{\pm} = -\sin \beta \phi_1^{\pm} + \cos \beta \phi_2^{\pm} \quad (8)$$

with mass  $m_{H^{\pm}} = \sqrt{\left( \frac{\mu_{12}}{v_1 v_2} - \frac{\lambda'_{12}}{2} \right) v^2}$ .

The CP-even scalar mass matrix in the  $(\rho_1 \ \rho_2 \ \rho_s)^T$  basis is given by

$$M_H^2 = \begin{pmatrix} 2\lambda_1 v_1^2 + \mu_{12} \frac{v_2}{v_1} & (\lambda_{12} + \lambda'_{12}) v_1 v_2 - \mu_{12} & \lambda_{1s} v_1 v_s \\ (\lambda_{12} + \lambda'_{12}) v_1 v_2 - \mu_{12} & 2\lambda_2 v_2^2 + \mu_{12} \frac{v_1}{v_2} & \lambda_{2s} v_2 v_s \\ \lambda_{1s} v_1 v_s & \lambda_{2s} v_2 v_s & 2\lambda_s v_s^2 \end{pmatrix}, \quad (9)$$

In general, the determinant of the mass matrix of CP-even scalar is non-zero, which tells us that there will be three massive CP-even scalars after the symmetry breaking. We identify the three CP-even mass eigenstates as  $h_1, h_2$  and  $h_3$ . They are linear combinations of the flavour states and can be written as

$$h_i = Z_{ij}^h \rho_j, \quad (10)$$

where  $Z_{ij}^h$  represents the mixing matrix for the CP-even states.

For our analysis, we hereafter denote  $h_1, h_2$  and  $h_3$  as the physical eigenstates in ascending order of their masses. For simplicity, we restrict our choice on the parameters in the scalar sector such that the lowest mass eigenstate among all scalars will be the 125 GeV scalar, identified as the SM Higgs boson observed at the experiments. As we do not consider a full analysis of the scalar sector in this work, it helps us to focus solely on the  $Z'$  and heavy neutrinos of the model. The other two CP-even states are taken to be beyond 700 GeV. As the properties of the lightest scalar must be similar to the SM Higgs boson, we choose the parameters such that  $h_1$  belongs mainly to the first Higgs doublet  $H_1$ . In terms of the mixing matrix components  $|Z_{11}^h|^2 \simeq 1$ . This natural choice is easily achieved if the diagonal entries of mass matrix  $M_H^2$  are much larger compared to the off-diagonal entries. This choice also suggests that  $v_1 \simeq v$ , which implies that  $\tan \beta \ll 1$ . We discuss the choice of  $\tan \beta$  further in section II C. In this setup, the three diagonal entries are controlled by  $v_1, \mu_{12}$ , and  $v_s$ . So, the mass of the heavy scalars will be given (to an approximation) by  $m_{h_2} \simeq \sqrt{\mu_{12} \cot \beta}$ , and  $m_{h_3} \simeq \sqrt{2\lambda_s v_s^2}$ . The mass for the charged scalar as well as the pseudo-scalar will also be similar to the mass of  $h_2$ .

## B. Gauge kinetic mixing and masses of gauge bosons

The presence of two or more  $U(1)$  gauge group in a theory allows us to write a gauge kinetic mixing term between the two  $U(1)$  gauge bosons without spoiling the gauge invariance of the Lagrangian [29]. The kinetic term for the gauge bosons in the Lagrangian, after including the gauge kinetic mixing, then becomes

$$\mathcal{L} \supset -\frac{1}{4}G^{a,\mu\nu}G_{\mu\nu}^a - \frac{1}{4}W^{b,\mu\nu}W_{\mu\nu}^b - \frac{1}{4}B^{\mu\nu}B_{\mu\nu} - \frac{1}{4}C^{\mu\nu}C_{\mu\nu} + \frac{1}{2}\tilde{g}B^{\mu\nu}C_{\mu\nu}, \quad (11)$$

where  $\tilde{g}$  is the kinetic mixing parameter. The following field redefinitions make the kinetic term diagonal with desired coefficient

$$B^\mu = B'^\mu + \frac{\tilde{g}}{\sqrt{1-\tilde{g}^2}}C'^\mu, \quad (12)$$

$$C^\mu = \frac{1}{\sqrt{1-\tilde{g}^2}}C'^\mu. \quad (13)$$

The field redefinition tells us that  $\tilde{g}$  should be less than 1 for the fields to be real. This is usually referred to as the ‘theoretical constraint’ on  $\tilde{g}$ . After achieving the correct form for

the gauge kinetic term with the above field redefinitions, we can now try to write the mass terms of gauge bosons arising from the kinetic terms of the scalars,

$$\mathcal{L}_{m,\text{gauge}} = (D^\mu \langle H_1 \rangle)^\dagger D_\mu \langle H_1 \rangle + (D^\mu \langle H_2 \rangle)^\dagger D_\mu \langle H_2 \rangle + (D^\mu \langle S \rangle)^\dagger D_\mu \langle S \rangle, \quad (14)$$

where

$$\langle H_1 \rangle = \begin{pmatrix} \frac{v_1}{\sqrt{2}} \\ 0 \end{pmatrix}, \quad \langle H_2 \rangle = \begin{pmatrix} \frac{v_2}{\sqrt{2}} \\ 0 \end{pmatrix}, \quad \langle S \rangle = \frac{v_s}{\sqrt{2}} \quad (15)$$

with the gauge covariant derivatives for the corresponding scalars defined as

$$D_\mu^{(1)} = \partial_\mu - ig_2 \frac{\sigma^a}{2} W_\mu^a + i \frac{g_1}{2} B_\mu, \quad (16)$$

$$D_\mu^{(2)} = \partial_\mu - ig_2 \frac{\sigma^a}{2} W_\mu^a + i \frac{g_1}{2} B_\mu + ig_x q_x C_\mu, \quad (17)$$

$$D_\mu^{(S)} = \partial_\mu - 2ig_x q_x C_\mu. \quad (18)$$

The  $U(1)_X$  charges of all the fields are proportional to  $q_x$ . In a gauge theory, the gauge coupling always comes with the gauge charges, *i.e.* the constant that we will see is  $g_x q_x$ . This means that we can absorb  $q_x$  in  $g_x$ . So, we will take  $q_x = 1$  henceforth. With the VEVs as defined in Eq. (15), we get mass terms for the gauge bosons as follows:

$$\begin{aligned} \mathcal{L}_{m,\text{gauge}} &= \frac{1}{4} \left| \begin{pmatrix} g_2 W_\mu^3 - g_1 B_\mu & g_2 (W_\mu^1 - i W_\mu^2) \\ g_2 (W_\mu^1 + i W_\mu^2) & -g_2 W_\mu^3 - g_1 B_\mu \end{pmatrix} \begin{pmatrix} \frac{v_1}{\sqrt{2}} \\ 0 \end{pmatrix} \right|^2 \\ &\quad + \frac{1}{4} \left| \begin{pmatrix} g_2 W_\mu^3 - g_1 B_\mu - 2g_x C_\mu & g_2 (W_\mu^1 - i W_\mu^2) \\ g_2 (W_\mu^1 + i W_\mu^2) & -g_2 W_\mu^3 - g_1 B_\mu - 2g_x C_\mu \end{pmatrix} \begin{pmatrix} \frac{v_2}{\sqrt{2}} \\ 0 \end{pmatrix} \right|^2 + 2g_x^2 v_s^2 C_\mu C^\mu \\ &= \frac{1}{4} g_2^2 v^2 W_\mu^+ W^{-\mu} + \frac{1}{8} v_1^2 \left| \left( g_2 W_\mu^3 - g_1 B'_\mu - \frac{g_1 \tilde{g}}{\sqrt{1 - \tilde{g}^2}} C'_\mu \right) \right|^2 \\ &\quad + \frac{1}{8} v_2^2 \left| \left( g_2 W_\mu^3 - g_1 B'_\mu - \frac{g_1 \tilde{g}}{\sqrt{1 - \tilde{g}^2}} C'_\mu - \frac{2g_x}{\sqrt{1 - \tilde{g}^2}} C'_\mu \right) \right|^2 + \frac{2g_x^2 v_s^2}{(1 - \tilde{g}^2)} C'_\mu C'^\mu. \end{aligned}$$

From Eq. (13), we see that  $C'_\mu$  is always accompanied by the factor  $\frac{1}{\sqrt{1 - \tilde{g}^2}}$ . Since the coupling  $g_x$  always comes with  $C_\mu$ , and hence with  $C'_\mu$ , we may absorb this extra factor inside  $g_x$ . Also, from the above equation, we see that  $\tilde{g}$  does not appear separately. Hence, without loss of generality, we do the following redefinitions in the coupling in order to get simplified expressions

$$g'_x = \frac{g_1 \tilde{g}}{\sqrt{1 - \tilde{g}^2}}, \quad g_x \rightarrow g_x \sqrt{1 - \tilde{g}^2}. \quad (19)$$



In Eq. (19), the last redefinition means that we replace  $g_x$  by  $g_x\sqrt{1-\tilde{g}^2}$  in each place in the Lagrangian. We should also note that there is no restriction on  $g'_x$  from theoretical constraint even though we had restrictions on  $\tilde{g}$ .

The mass matrix for the neutral gauge bosons, in the basis of  $(B'_\mu \ W_\mu^3 \ C'_\mu)^T$  is given by

$$M^2 = \frac{1}{4} \begin{pmatrix} g_1^2 v^2 & -g_1 g_2 v^2 & g_1 (g'_x v^2 + 2g_x v_2^2) \\ -g_1 g_2 v^2 & g_2^2 v^2 & -g_2 (g'_x v^2 + 2g_x v_2^2) \\ g_1 (g'_x v^2 + 2g_x v_2^2) & -g_2 (g'_x v^2 + 2g_x v_2^2) & g_x'^2 v^2 + 4g_x g'_x v_2^2 + 4g_x^2 (v_2^2 + 4v_s^2) \end{pmatrix} \quad (20)$$

The diagonalization of the mass matrix of the neutral gauge bosons can be done in the following way,

(i) First we rotate  $W_\mu^3$  and  $B'_\mu$  to get  $A_\mu$  and  $X_\mu$ .

$$\begin{pmatrix} A_\mu \\ X_\mu \\ C'_\mu \end{pmatrix} = \begin{pmatrix} \cos \theta_W & \sin \theta_W & 0 \\ -\sin \theta_W & \cos \theta_W & 0 \\ 0 & 0 & 1 \end{pmatrix} \begin{pmatrix} B'_\mu \\ W_\mu^3 \\ C'_\mu \end{pmatrix}, \quad (21)$$

where  $\tan \theta_W = \frac{g_1}{g_2}$ . The mass term for neutral gauge boson then becomes

$$\mathcal{L}_{m,\text{gauge}} = \frac{1}{8} v_1^2 (g_z X_\mu - g'_x C'_\mu)^2 + \frac{1}{8} v_2^2 (g_z X_\mu - (g'_x + 2g_x) C'_\mu)^2 + 2g_x^2 v_s^2 C'_\mu C'^\mu, \quad (22)$$

where  $g_z = \sqrt{g_1^2 + g_2^2}$ . The above expression does not have any mass term for  $A_\mu$ . This means  $A_\mu$  is massless, which can be identified as photon. The angle  $\theta_W$  can be identified as the Weinberg angle as we get in the SM.

(ii) Now, the mass matrix of  $X_\mu$  and  $C'_\mu$  is given by

$$\widetilde{M}^2 = \frac{1}{4} \begin{pmatrix} g_z^2 v^2 & -g_z (g'_x v^2 + 2g_x v_2^2) \\ -g_z (g'_x v^2 + 2g_x v_2^2) & g_x'^2 v^2 + 4g_x g'_x v_2^2 + 4g_x^2 (v_2^2 + 4v_s^2) \end{pmatrix}. \quad (23)$$

The above mass matrix can be diagonalized by the orthogonal transformation between  $X_\mu$  and  $C'_\mu$  as follows

$$\begin{pmatrix} Z_\mu \\ Z'_\mu \end{pmatrix} = \begin{pmatrix} \cos \theta' & \sin \theta' \\ -\sin \theta' & \cos \theta' \end{pmatrix} \begin{pmatrix} X_\mu \\ C'_\mu \end{pmatrix}, \quad (24)$$

where

$$\tan 2\theta' = \frac{2g_z(g'_x v^2 + 2g_x v_2^2)}{g_x'^2 v^2 + 4g_x g'_x v_2^2 + 4g_x^2(v_2^2 + 4v_s^2) - g_z^2 v^2}. \quad (25)$$

After the diagonalization, the mass of the physical gauge bosons are

$$M_{Z,Z'}^2 = \frac{1}{8} \left[ g_z^2 v^2 + g_x'^2 v^2 + 4g_x g'_x v_2^2 + 4g_x^2(v_2^2 + 4v_s^2) \right] \pm \frac{1}{8} \sqrt{\left( g_x'^2 v^2 + 4g_x g'_x v_2^2 + 4g_x^2(v_2^2 + 4v_s^2) - g_z^2 v^2 \right)^2 + 4g_z^2 \left( g'_x v^2 + 2g_x v_2^2 \right)^2}, \quad (26)$$

and the final mixing matrix becomes

$$\begin{pmatrix} B_\mu \\ W_\mu^3 \\ C_\mu \end{pmatrix} = \begin{pmatrix} \cos \theta_W & -\sin \theta_W \cos \theta' + \frac{g'_x}{g_1} \sin \theta' & \sin \theta_W \sin \theta' + \frac{g'_x}{g_1} \cos \theta' \\ \sin \theta_W & \cos \theta_W \cos \theta' & -\cos \theta_W \sin \theta' \\ 0 & \sin \theta' \frac{\sqrt{g_1^2 + g_x'^2}}{g_1} & \cos \theta' \frac{\sqrt{g_1^2 + g_x'^2}}{g_1} \end{pmatrix} \begin{pmatrix} A_\mu \\ Z_\mu \\ Z'_\mu \end{pmatrix} \quad (27)$$

Note that the mixing between the  $Z$  and  $Z'$  needs to be quite small such that it does not modify the  $Z$  boson couplings with the SM fields. In order to study the parameters that would be most relevant in establishing the  $Z$ - $Z'$  mixing, we look at Eq. 25 in more detail. We find that the kinetic mixing dictates that the coefficient  $g'_x$  appears with the SM VEV while the  $U(1)_X$  coupling  $g_x$  appears with the VEV of the second scalar doublet in the numerator of Eq. (25). Assuming that the kinetic mixing coefficient and the  $U(1)_X$  gauge coupling are of the same order, one can approximate Eq. (25) depending on the choice of  $\tan \beta$ . Note that for  $\tan \beta \ll 1$ , i.e.  $v_1 \simeq v$ , the dominant term in the numerator becomes proportional to  $g_z g'_x v_1^2$  while for  $\tan \beta \gg 1$ , i.e.  $v_2 \simeq v$ , the dependence is on  $g_z(2g_x + g'_x)v_2^2$ . The denominator can be easily approximated to a form  $(M_{Z'}^2 - M_Z^2)$  in either case, provided  $v_s \gg v_1, v_2$ . Thus depending on the choice of  $\tan \beta$ , we expect the mixing angle to vary for different ranges of  $g'_x$  and  $g_x$  values.

To highlight the case where  $\tan \beta > 1$ , i.e.  $v_2 > v_1$ , we scan over a range of values for  $g'_x$  and  $g_x$  as well as  $v_s$  for  $1 < \tan \beta < 60$  and calculate the mixing angle  $\theta'$ . In Fig. 1, we show the dependence of the  $Z$ - $Z'$  mixing angle ( $\theta'$ ), as a function of  $M_{Z'}$  along with its dependence on the variation of the gauge kinetic mixing ( $g'_x$ ). Note that for large values of  $M_{Z'} > 1$  TeV the denominator term is significantly large and therefore the mixing angle is naturally small. However the numerator in Eq. (25) is proportional to  $g_z(2g_x + g'_x)v_2^2$  for  $\tan \beta \gg 1$  and we find that even with the kinetic mixing vanishing, the mixing angle

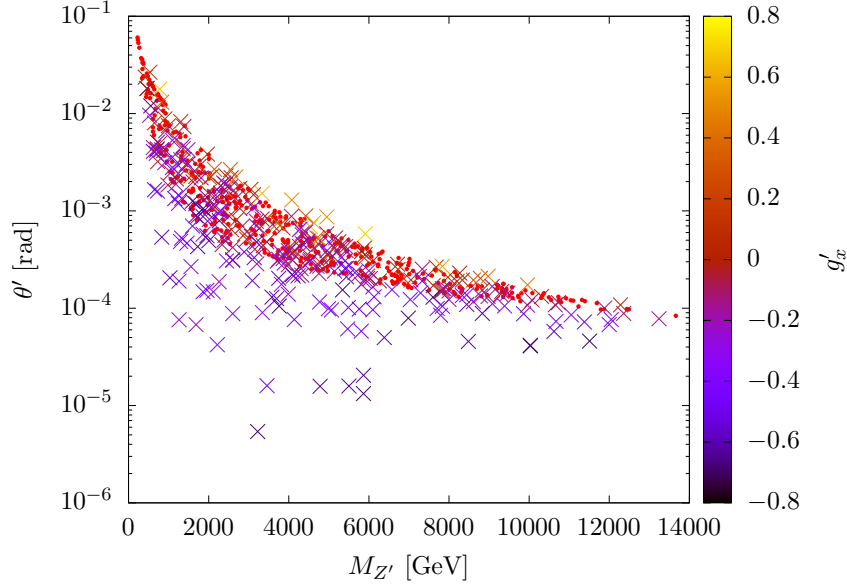


FIG. 1.  $(M_{Z'}, \theta')$  along with the gauge kinetic mixing  $g'_x$  on the colour bar. Red points refer to  $g'_x = 0$  while cross symbols 'x' indicate the non-vanishing  $g'_x$ . Here the scan is carried out for parameter values in the range  $1 \leq v_s \leq 10$  TeV,  $0.1 \leq g_x \leq 0.7$  and  $-1 \leq g'_x \leq 1$ .

has values larger than  $\mathcal{O}(10^{-2})$  for  $M_{Z'} < 750$  GeV. This is expected as the denominator  $(M_{Z'}^2 - M_Z^2)$  becomes smaller, while  $g_x$  is non-vanishing and constrained by the  $Z'$  mass. This gives an interesting result that, even with vanishing kinetic mixing, if the  $Z'$  gets a part of its mass from the scalar doublet, it leads to a substantial  $Z$ - $Z'$  mixing which would disfavour the parameter space due to strong constraints from  $Z$  boson measurements. However it is still possible to obtain small  $\theta' < 10^{-3}$  for the light  $Z'$  case, provided there is a cancellation in the numerator term  $\propto (2g_x + g'_x)$ . These are the points highlighted in the figure with crosses (x) corresponding to *negative* values of  $g'_x$ . Thus it is possible to obtain small  $Z$ - $Z'$  mixing compatible with  $Z$  boson data even for  $\tan \beta \gg 1$ . The stronger constraint on such a scenario however comes from Higgs data and perturbativity arguments which we discuss later along with the more favourable choice of parameter space where  $\tan \beta \ll 1$ .

### C. Masses and mixing of the charged lepton and quarks

The Lagrangian responsible for the masses and the mixing of leptons and quarks is essentially the Yukawa terms.

$$\mathcal{L} \supset -Y_l^{ij} \bar{l}_{Li} H_1^c e_{Rj} - Y_d^{ij} \bar{q}_{Li} H_1^c d_{Rj} - Y_u^{ij} \bar{l}_{Li} H_1 u_{Rj} + \text{h.c.} \quad (28)$$

The masses and the mixing can be arranged in the same way as it is done in the SM. The only difference is that the mass of the SM fermions are proportional to the VEV of  $H_1$ ,  $v_1$ . So, in order to achieve the correct mass, we need to choose Yukawa couplings  $Y_f = \frac{Y_f^{\text{SM}}}{\cos \beta}$ , where  $Y_f^{\text{SM}} = \frac{\sqrt{2}m_f}{v}$  is the value of the respective Yukawa couplings in the SM. This choice also ensures that the Cabibo-Kobayashi-Maskawa (CKM) matrix remains the same as the SM. With this choice, we tabulate the couplings of the fermions to the scalars, namely  $h_i$  ( $i = 1, 2, 3$ ),  $A$  and  $H^\pm$ , in Table II. In order to maintain perturbativity of all the couplings, we need to keep these coupling below  $\sqrt{4\pi}$ . From the table, it is clear that the natural choice for  $\tan \beta$  is smaller values. The strongest constraint from perturbativity comes from the top quark since it is the heaviest fermion in the SM. In the case of top quark,  $\sqrt{2}\frac{m_f}{v} \simeq 1$ . Hence, if we take  $Z_{i1}^h \simeq 1$ ,  $\tan \beta$  should be such that  $\cos \beta > \frac{1}{\sqrt{4\pi}}$  from perturbativity consideration. This gives, although an approximate one, an upper bound of  $\tan \beta < 3$ . With this bound in mind we shall restrict our study to values of  $\tan \beta < 1$  for further analysis. Recall that for any value of  $\tan \beta > 1$ , there is significant increase in the couplings of the SM fermions with the scalars in the model. A critical scrutiny of its implications and phenomenology for the scalar sector in the current model is left for future work and we focus on the  $Z'$  signal in this work.

Couplings for	$h_i - f - \bar{f}$	$A - f - \bar{f}$	$H^\pm - f - \bar{f}'$
$g_f$	$Y_f^{\text{SM}} \frac{Z_{i1}^h}{\cos \beta}$	$Y_f^{\text{SM}} \tan \beta$	$Y_f^{\text{SM}} \tan \beta$

TABLE II. The coupling of the fermions with different scalars of the model.

#### D. Masses of neutrinos

In this model, we give Majorana masses to the neutrinos via inverse sea-saw mechanism [30–32]. We re-write the relevant part of the Lagrangian below.

$$\mathcal{L} \supset - Y_\nu \bar{l}_L H_2 N_R - Y_R S \bar{N}_R N_R^C - Y_L S \bar{N}_L N_L^C - \hat{M}_N \bar{N}_L N_R + \text{h.c.} \quad (29)$$

We have added 3-generations of sterile neutrinos ( $N_R^i$  and  $N_L^i$ ) corresponding to the 3-generations of fermion in the SM which renders all the Yukawa couplings ( $Y_\nu$ ,  $Y_L$  and  $Y_R$ ) as  $3 \times 3$  matrices. Note that the two chiral states  $N_R$  and  $N_L$  combine to form a vector-like fermion ( $\hat{N}$ ) which is a singlet under SM and carries the same  $U(1)_X$  charge as its chiral

components. After symmetry breaking, the mass term for the neutrinos are given by

$$\mathcal{L}_\nu^{\text{mass}} = -\frac{v_2}{\sqrt{2}}Y_\nu\bar{\nu}_L N_R - \frac{v_s}{\sqrt{2}}Y_R\bar{N}_R^C N_R - \hat{M}_N\bar{N}_L N_R - \frac{v_s}{\sqrt{2}}Y_L\bar{N}_L^C N_L + \text{h.c.} \quad (30)$$

The mass matrix in  $(\nu_L \ N_R^C \ N_L)^T$  basis is given by

$$\mathcal{M}_\nu = \begin{pmatrix} 0 & m_D^T & 0 \\ m_D & m_R & \hat{M}_N \\ 0 & \hat{M}_N^T & m_L \end{pmatrix}, \quad (31)$$

where  $m_D = v_2 Y_\nu / \sqrt{2}$ ,  $m_R = \sqrt{2} v_s Y_R$  and  $m_L = \sqrt{2} v_s Y_L$ . Also,  $m_L$  and  $m_R$  are naturally small due to the so-called 't Hooft criteria [33]. Indeed, in the limit  $m_{L,R} \rightarrow 0$ , the lepton number is restored as a conserved symmetry.

As mentioned above,  $m_L, m_R \ll m_D, \hat{M}_N$ , thus the neutrino masses can be given, with a very good approximation, by

$$m_{\nu_\ell} \simeq \frac{m_D^2 m_L}{\hat{M}_N^2 + m_D^2}, \quad (32)$$

$$m_{\nu_{H,H'}} \simeq \frac{1}{2} \left( \frac{\hat{M}_N^2 m_L}{\hat{M}_N^2 + m_D^2} + m_R \right) \mp \sqrt{\hat{M}_N^2 + m_D^2}. \quad (33)$$

It is worth mentioning that in this scenario, the neutrino Yukawa coupling  $Y_\nu$ , can be of order  $\mathcal{O}(0.1)$  and the large scale  $\hat{M}_N$  can lie in the range of a few hundred GeV–TeV. This is because the suppression factor needed to account for light neutrino masses are played by the naturally small parameters  $m_L$  instead of the Yukawa coupling  $Y_\nu$ . Such a large Yukawa coupling plays a crucial role for producing these heavy neutrinos (which are complete SM isosinglets) at experiments directly through SM mediators and helps in testing these type of models and probing the heavy neutrino physics at colliders (some examples as in Refs. [34–38]). Indeed, if  $Y_\nu \sim \mathcal{O}(0.1)$ ,  $\hat{M}_N \sim 1$  TeV and  $m_L \sim \mathcal{O}(10^{-6})$  GeV, then an order of  $\mathcal{O}(0.1)$  eV neutrino mass can be obtained.

The light neutrino mass matrix in Eq. (32) must be diagonalized by the physical neutrino mixing matrix  $U_{\text{PMNS}}$  [39] *i.e.*,

$$U_{\text{PMNS}}^T m_{\nu_\ell} U_{\text{PMNS}} = m_{\nu_\ell}^{\text{diag}} \equiv \text{diag}\{m_{\nu_e}, m_{\nu_\mu}, m_{\nu_\tau}\}. \quad (34)$$

Thus, one can easily show that the Dirac neutrino mass matrix can be defined as :

$$m_D = U_{\text{PMNS}} \sqrt{m_{\nu_\ell}^{\text{diag}}} R \sqrt{m_L^{-1}} \hat{M}_N, \quad (35)$$

where  $R$  is an arbitrary orthogonal matrix. Accordingly, the  $(9 \times 9)$  neutrino mass matrix  $\mathcal{M}_\nu$  can be diagonalized by  $\mathcal{N}$ , *i.e.*,  $\mathcal{N}\mathcal{M}_\nu\mathcal{N}^\dagger = \mathcal{M}_\nu^{\text{diag}}$ , which is given by [40]

$$\mathcal{N} = \begin{pmatrix} \mathcal{N}_{3 \times 3} & \mathcal{N}_{3 \times 6} \\ \mathcal{N}_{6 \times 3} & \mathcal{N}_{6 \times 6} \end{pmatrix}, \quad (36)$$

where

$$\mathcal{N}_{3 \times 3} \simeq \left(1 - \frac{1}{2}F^2\right) U_{\text{PMNS}}, \quad \mathcal{N}_{3 \times 6} = (\mathbf{0}_{3 \times 3}, F) \mathcal{N}_{6 \times 6}, \quad F = m_D \hat{M}_N^{-1}. \quad (37)$$

It is clear that the deviation of a non-unitary matrix  $\mathcal{N}_{3 \times 3}$  from the standard  $U_{\text{PMNS}}$  is measured by the size of  $\frac{1}{2}F^2$ . Also, the muon  $g - 2$  anomaly and the lepton flavor violating processes can be affected by the  $F$  size [41]. Consequently, that imposes upper bounds on  $F$  entries to be small [42–44], which is automatically satisfied in our model due to the smallness of  $v_2$  (*i.e.*,  $v_1 \simeq v$ ).

In normal hierarchy scenario, *i.e.*, assuming  $m_{\nu_1} \ll m_{\nu_2} < m_{\nu_3}$ , the two mass square differences determined from the oscillation data [45] is given by  $\Delta m_{21}^2 = (7.05 - 8.24) \times 10^{-5} \text{ eV}^2$  and  $\Delta m_{31}^2 = (2.334 - 2.524) \times 10^{-3} \text{ eV}^2$ . Therefore, there are at least two non-zero  $m_{\nu_i}$ . Assuming the lightest neutrino to be massless, we get  $m_{\nu_i} \simeq (0, 8.66 \times 10^{-3}, 0.05) \text{ eV}$ .

In normal hierarchy scenario,  $m_{\nu_1} < m_{\nu_2} < m_{\nu_3}$ , the two mass square differences determined from the oscillation data [45] is given by  $\Delta m_{21}^2 = (7.05 - 8.24) \times 10^{-5} \text{ eV}^2$  and  $\Delta m_{31}^2 = (2.334 - 2.524) \times 10^{-3} \text{ eV}^2$ . Therefore, there are at least two non-zero  $m_{\nu_i}$ . Assuming the lightest neutrino to be massless, we get  $m_{\nu_i} \simeq (0, 8.66 \times 10^{-3}, 0.05) \text{ eV}$ .

For simplicity, we assumed  $Y_\nu, \hat{M}_N$  to be diagonal and  $Y_\nu^{ii} = y_\nu, \hat{M}_N^{ii} = m_N, i = 1, 2, 3$ , and  $Y_R = 0$ . Also, we defined  $y_L = Y_L^{22} = Y_L^{33} \sqrt{\Delta m_{21}^2 / \Delta m_{31}^2}$ . In Fig. 2, we show the allowed  $y_\nu$  and  $y_L$  ranges to satisfy the central values of the difference of neutrino masses-squared ( $\Delta m_{21}^2, \Delta m_{31}^2$ ) for three different values of  $m_N = 250 \text{ GeV}, 500 \text{ GeV}, 1000 \text{ GeV}$  (left panel), where the solid (dashed) curves refer to  $\tan \beta = 0.01(3)$  and in the right panel we show the same but for different values of  $\tan \beta = 0.01, 0.1, 1, 3$  with  $m_N$  fixed at  $500 \text{ GeV}$ .

### III. EXPERIMENTAL CONSTRAINTS

The extension to the SM considered in this model affects the three sectors of the SM, *viz.* (a) scalar sector, (b) neutrino sector, and (c) neutral gauge boson sector. We therefore need

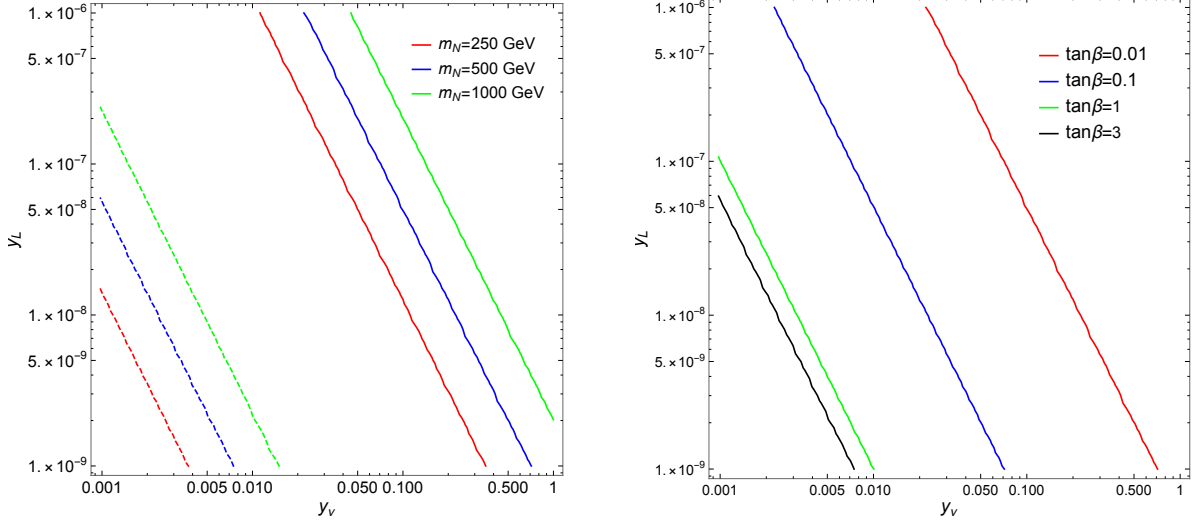


FIG. 2.  $(y_\nu, y_L)$  plane in which the all curves satisfy the central values of the difference of neutrino masses-squared ( $\Delta m_{21}^2$ ,  $\Delta m_{31}^2$ ).

to focus on each of these to evaluate the experimental constraints that affect the parameter space of the model.

### A. Properties of the $Z$ boson

Due to the mixing of the gauge bosons, the coupling of  $Z$  boson to SM particles gets modified with respect to that of the SM. As a result, the total decay width of the  $Z$  boson as well as its partial decay width to light neutrinos (which mix with the heavy neutrinos) is also modified. The modification in all the couplings besides the neutrinos is approximately proportional to  $\sin \theta'$  (the  $Z$ - $Z'$  mixing parameter). The  $Z$  boson properties have been measured at LEP with great precision and any changes to its decay properties result in the limit for  $\theta' \lesssim 10^{-3}$  [39]. This restriction puts a very strong constraint on the parameter space (*viz.* Eq. (25)). In order to respect the constraints arising from the properties of the  $Z$  boson, we choose the parameters of our model such that  $\theta' < 10^{-3}$  is satisfied. As one can see from Eq. (25), the value of  $\theta'$  depends on the coupling  $g_x$  and gauge kinetic mixing  $g'_x$  as well as the value of the EW VEVs *viz.*  $\tan \beta = \frac{v_2}{v_1}$  and  $v_s$ . As pointed out earlier, for high values of  $v_s$  leading to  $M_{Z'} > 1$  TeV, this bound is easily satisfied. Again, for  $\tan \beta > 1$  we already discussed the regions of parameter space that is allowed for lower mass of  $Z'$  in the concluding part of Sec. II B. Our interest lies in the parameter space with the more

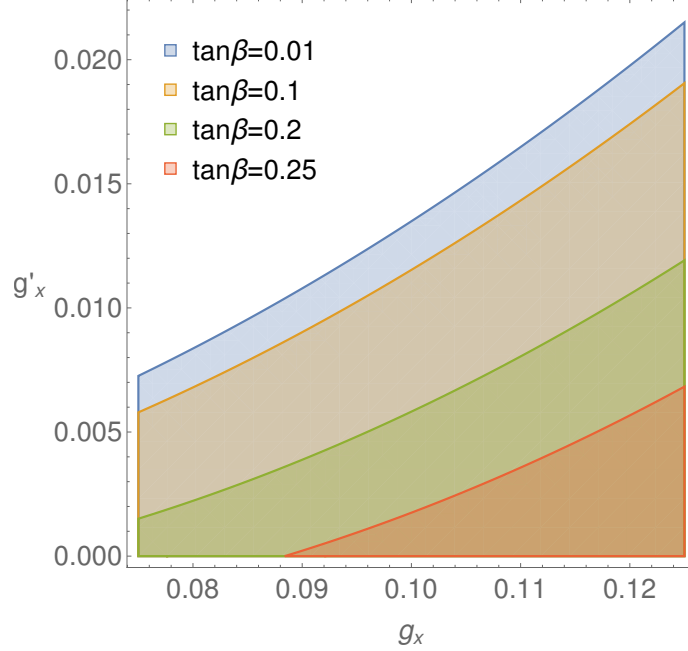


FIG. 3. Illustration of allowed region satisfying  $\theta' \leq 10^{-3}$  in  $g_x - g'_x$  plane for  $v_s = 2$  TeV for four different value of  $\tan \beta$ .

compatible choice of  $\tan \beta < 1$  which allows a lighter  $Z'$ .

In Fig. 3, we show the allowed region in the  $g_x - g'_x$  plane for  $v_s = 2$  TeV for different values of  $\tan \beta$  less than one. The range of  $g_x$  is chosen such that the mass of  $Z'$  remains within 200–500 GeV. As the mass of the  $Z'$  is approximated by  $M_{Z'} \sim 2 g_x v_s$ , the value of  $M_{Z'}$  within a certain range allows us to fix  $g_x$  appropriately for a fixed value of  $v_s$ . As pointed out earlier, for  $\tan \beta \ll 1$  we have the numerator in Eq. (25) proportional to the product of  $g'_x$  and  $v_1^2$ . Thus, for  $g'_x = 0$ , even a  $g_x \sim \mathcal{O}(1)$  is allowed for the  $U(1)_X$  gauge coupling. Thus, substantially large values of  $g_x$  is allowed even when the  $Z'$  mass lies between 200–500 GeV, restricted only by the choice of  $v_s$ . This possibility leads us to the choice of the coupling which allows the  $Z'$  to decay dominantly to a pair of the heavy neutrinos (when kinematically allowed) while all other modes are suppressed. We will see that this also helps us evade existing collider limits on light  $Z'$ .

## B. Higgs Signals and Higgs Bounds

The introduction of another Higgs doublet and singlet modifies the scalar sector. The modifications are of the following two forms.



- Due to the mixing between scalars, the production and branching fraction of the observed 125 GeV scalar gets modified with respect to the SM Higgs. These properties are measured in terms of signal strength of Higgs which gives constraint on the parameters [46–53].
- The model predicts heavy scalars which may be observed at the LHC. However, the LHC did not observe any new scalar other than the 125 GeV one. This gives another constraints on the production of any new scalars.

Note that the choice of small  $\tan\beta$  leads to suppressed couplings of charged scalars and pseudo-scalar to the fermions as can be seen from the couplings shown in Table II. As a result, the production of these scalars at a collider are significantly suppressed. This helps us to evade any bounds coming from non-observation of such scalar at the LHC. However, the coupling of CP-even scalars ( $h_i$ ) to the fermions are not all suppressed due to the small values of  $\tan\beta$ . These couplings are mainly dictated by the entries in the CP-even scalar mixing matrix given by  $Z_{i1}^h$ . Since we demand that the 125 GeV scalar belongs mainly to the  $H_1$  doublet, we restrict ourselves to  $Z_{11}^h \simeq 1$  and  $Z_{21}^h, Z_{31}^h \ll 1$ . This leads to suppressed production rates for the two heavy CP-even scalars while ensuring that the properties of the 125 GeV scalar ( $h_1$ ) resembles the SM Higgs.

Although we do not explore the Higgs sector of the model in this article, we need to ensure that the parameter choice for the scalar sector satisfies all relevant constraints including that of the observed Higgs boson mass and its decay probabilities. To achieve this we use the publicly available packages, **HiggsSignals** [54] and **HiggsBounds** [55, 56] in our scan of the parameter space to check for compatible points. These two packages incorporate the constraints of Higgs signal strength of the 125 GeV scalar and also check the existing limits on the heavy scalars (at 95% C.L.). We shall henceforth fix the scalar sector parameters and masses consistent with relevant experimental constraints. The parameter choices and the corresponding scalar masses are shown in Table III.

$\lambda_1$	$\lambda_2$	$\lambda_3$	$\lambda_4$	$\lambda_{1s}$	$\lambda_{2s}$	$\mu_{12}$ (GeV <sup>2</sup> )	$\tan\beta$	$m_{h_1}$ (GeV)	$m_{h_2}$ (TeV)	$m_{H^\pm}$ (GeV)	$m_A$ (TeV)
0.1289	1.0	0.005	0.005	0.0	−0.5	$10^4$	0.01	125.0	1.0	999.9	1.0

TABLE III. Scalar sector parameters and masses consistent with all experimental constraints.

The only parameter that we do vary in the scalar sector when we fix the benchmark

points for our analysis would be the singlet VEV  $v_s$  and the corresponding quartic term coefficient  $\lambda_s$ , which will affect the  $Z'$  and  $h_3$  masses.

### C. Search for new $Z'$ gauge boson

The phenomenology of  $Z'$  in the model is quite different from that of the more traditional  $U(1)$  extensions. In the absence of gauge kinetic mixing, the coupling of  $Z'$  to the SM fermions gets modified by an additive factor proportional to  $\sin \theta'$ , which has to be small to be consistent with the measurement of  $Z$  boson properties. However, the introduction of kinetic mixing parametrized by  $g'_x$ , we have an additional part in coupling which is proportional to  $g'_x \cos \theta'$ . We have listed the expression for the coupling of the  $Z'$  with the matter fields of the model in the appendix for reference.

As none of the SM fields are charged under the new  $U(1)$ , the  $Z'$  couples to the SM charged fermions only via the  $Z$ - $Z'$  mixing. For  $\tan \beta > 1$  we found that the mixing angle was dependent on both  $g_x$  and  $g'_x$ . A small  $\theta' \lesssim 10^{-3}$  for  $M_{Z'}$  in the range of 200–500 GeV required a cancellation such that  $g'_x \simeq -2g_x$ . However, this choice would imply that the coupling of the  $Z'$  with the SM fermions and the new heavy neutrinos would have somewhat similar strength. Thus, in order to have substantial production cross-section, one also gets a substantial branching fraction of the  $Z'$  decay into SM fermions. For a light  $Z'$ , the strongest constraint from LHC comes from its decay into the di-lepton channel [27]. Evaluating this limit for the case  $\tan \beta > 1$ , puts a strong limit on the values of  $g'_x$  and  $g_x \sim 10^{-3}$ . Thus the promising search channel, when  $\tan \beta > 1$ , still remains the di-lepton mode, even with the heavy neutrino decay modes available for the  $Z'$ . In contrast, when we consider the more favourable option of  $\tan \beta < 1$ , we find that the constraint on  $\theta'$  is much more easily satisfied by suppressing the kinetic mixing parameter  $g'_x$  (even for light  $Z'$ ) while the decay modes of the gauge boson can be significantly tilted in favour of the new neutral fermions in the particle spectrum. However, a too suppressed  $g'_x$  would also suppress the production cross-section of the  $Z'$  at LHC, as can be seen by looking at its coupling with the SM quarks (appendix). We would therefore like to find a region of parameter space where the gauge boson is produced at LHC and leaves an observable imprint in final states still allowed by the LHC data.

We note that  $g'_x \lesssim 10^{-2}$  is sufficient to keep  $\theta' < 10^{-3}$ . This choice allows us to enhance

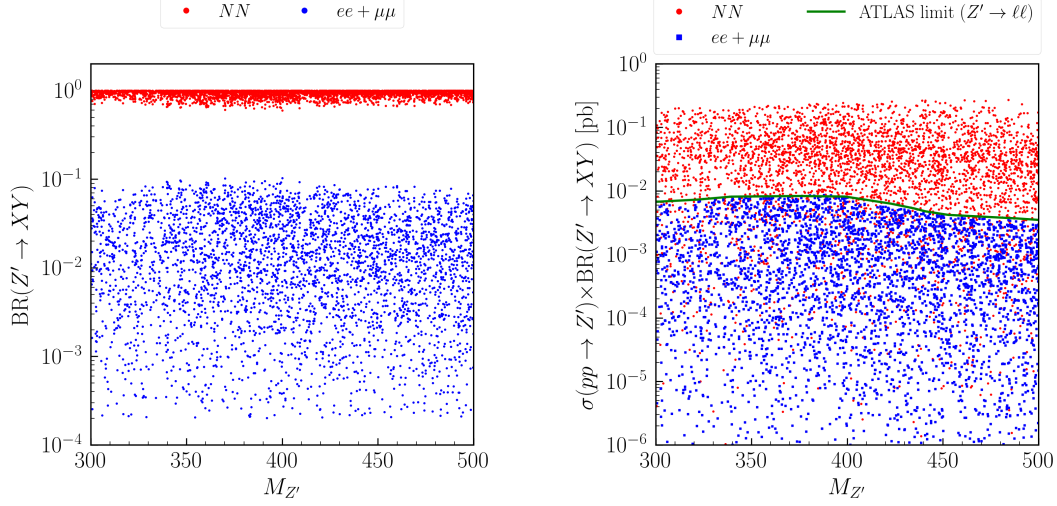


FIG. 4. (Left) Scatter plot of branching fraction of  $Z'$  to different decay channels. (Right) Scatter plot of  $\sigma(pp \rightarrow Z') \times \text{BR}(Z' \rightarrow XY)$  at 13 TeV LHC. The solid line in the plot represents the ATLAS upper bound on  $\sigma(pp \rightarrow Z') \times \text{BR}(Z' \rightarrow \ell^+ \ell^-)$  at 95% C.L. [27].

the production of  $Z'$  at a collider by four orders of magnitude, compared to the case when  $g'_x = 0$  where  $\sin \theta' \sim 10^{-5} - 10^{-6}$  (recall that  $\sin \theta'$  depends on  $g_x$  too). On the other hand, the coupling of  $Z'$  with the heavy neutrinos is mainly governed by the choice of  $g_x$ . From Fig. 3 we can see that the value of  $g_x$  can be taken to be  $\mathcal{O}(0.1)$  while maintaining all relevant bounds. If the mass of the heavy neutrino is less than  $M_{Z'}/2$  then  $Z'$  has an additional decay channel to a pair of heavy neutrinos. The decay to a pair of heavy neutrinos can be nearly 100% while all other modes become significantly suppressed. In such a case the  $\text{BR}(Z' \rightarrow \ell^+ \ell^-)$  can be reduced to values less than 1%. A scatter plot of the branching ratios of  $Z'$  to different decay channels has been shown in the left panel of Fig. 4. Here we have varied  $v_s$  between 1–10 TeV while  $g'_x$  is scanned over the range 0–0.02. On the right panel of the same figure, we show a scatter plot of  $\sigma(pp \rightarrow Z') \times \text{BR}(Z' \rightarrow XY)$  at 13 TeV LHC. The solid line in the plot represents the ATLAS upper bound on the  $\sigma(pp \rightarrow Z') \times \text{BR}(Z' \rightarrow \ell^+ \ell^-)$  where  $\ell = e, \mu$ . As one can clearly see, this interplay actually helps us to produce  $Z'$  at a higher rate while being within the bounds from the LHC in  $Z' \rightarrow \ell^+ \ell^-$  mode [27]. At the same time, we achieve a significantly high production cross-section of  $NN$  through the  $Z'$  resonance.

In Fig. 5, we show a scatter plot of points which satisfy all the three, *viz.* **HiggsSignals**, **HiggsBounds** and  $Z'$  search in  $\ell^+ \ell^-$  mode, in  $g_x - g'_x$  plane. The range for the scan over  $v_s$

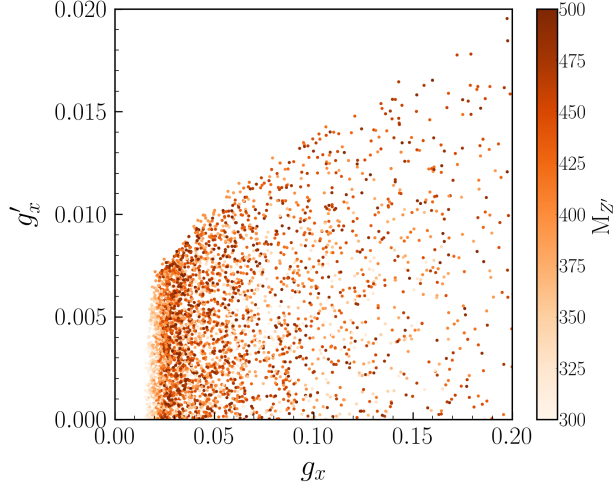


FIG. 5. Scatter plot of points satisfying all the three, *viz.* **HiggsSignals**, **HiggsBounds** and  $Z'$  search in  $\ell^+ \ell^-$  mode, in  $g_x - g'_x$  plane. The colour bar shows the variation of  $M_{Z'}$ .

and  $g'_x$  are the same as in Fig. 4. As expected, small  $g_x$  and  $g'_x$  values are always allowed as the constraint on  $\theta'$  and constraint from  $Z'$  searches are easily satisfied in that range of the parameter space. Since **HiggsBounds** and **HiggsSignals** limits do not have much dependence on  $g_x$  and  $g'_x$ , they put little constraint in this plane. Higher values of  $g'_x$  start getting disallowed since it leads to higher values for  $\theta' > 10^{-3}$ . However one finds that values of  $g_x$  in the range of  $0.01 - 0.2$  are allowed and  $g'_x \lesssim 0.1 g_x$  is sufficient to suppress the  $Z'$  decay to di-lepton mode to avoid the constraints from LHC, as can be seen in Figs. 3 and 4.

#### IV. COLLIDER ANALYSIS

We now look at the collider signatures for the new gauge boson  $Z'$  at LHC. The most obvious signal for a heavy  $Z'$  is via the Drell-Yan channel. In our scenario, the  $Z'$  couples to the SM sector mostly through the mixing parameter and  $g'_x$ . Therefore, the on-shell production rates of the  $Z'$  are crucially dependent on the  $\theta'$  which is also dependent on  $g'_x$ . For the gauge boson in the mass range of 200–500 GeV, constraints indicate  $\theta' \lesssim 10^{-3}$  which provides a significant limit to the production cross-section of  $\sigma(pp \rightarrow Z')$ . However the cleanliness of the di-lepton channel along with the resonant production of  $Z'$ <sup>1</sup> still provides a significantly strong constraint on  $Z'$  mass. This bound can be relaxed if the  $Z'$  decay to

<sup>1</sup> The small  $Z'$  width allows the use of Narrow-Width Approximation (NWA) in calculating the di-lepton cross-section using  $\sigma \times \text{BR}$ .

the charged lepton pair is suppressed, as shown in Fig. 4. The decay to a pair of heavy neutrinos opens up an interesting channel to search for  $Z'$  in this model. In addition we find that the upper bound on the production cross-section  $\sigma(pp \rightarrow Z')$  in this channel can be larger than what would be allowed in the absence of the  $Z' \rightarrow NN$  decay<sup>2</sup>. Thus we focus on the  $Z'$  signal through the pair production of heavy neutrinos via  $Z'$  resonance [57].

The dominant decay modes of  $N$  are  $\ell^\pm W^\mp$  and  $\nu Z$ . Since the heavy neutrinos are Majorana in nature,  $N$  can decay to leptons of either sign. This gives an interesting set of possibilities for final states. Depending on the decay modes of  $W^\pm$  and  $Z$ , we can have the following possibilities of final states.

- $4\ell + \cancel{E}_T$
- $3\ell + 2j + \cancel{E}_T$
- $2\ell + 4j + \cancel{E}_T$
- $4j + \cancel{E}_T$  (when only  $N \rightarrow \nu Z$  decay is considered.)

Although these are all interesting channels to look for  $Z'$  in this model, especially the same-sign di-lepton (SSDL) with jets and missing transverse energy (MET), we mainly focus on the more sensitive 4-lepton and 3-lepton signals with smaller SM background in this article. Studies in the multi-lepton channels including the SSDL mode for heavy neutrinos produced via  $Z'$  has always been of interest, and has been looked at before [57–63].

For our analysis of the trilepton and four lepton channels, we have chosen three benchmark points. The values of the important parameters of these three benchmark points are tabulated in Table IV. Note that the slight variation in the values of  $v_s$  for the three benchmark points are made to adjust the  $Z'$  mass to their respective values chosen for the analysis. The leading-order (LO) production cross-section of  $Z'$  at the 14 TeV LHC run machine and branching ratios of  $Z' \rightarrow NN$  for these three benchmark points are also mentioned in the table. Note that for  $M_N > M_{Z'}/2$ , the branching probability of  $\text{BR}(Z' \rightarrow ee + \mu\mu) \sim 28\%$  constraining the allowed upper bound for  $g'_x$  to become  $2.48 \times 10^{-3}$ ,  $4.58 \times 10^{-3}$  and  $4.44 \times 10^{-3}$  for the three benchmark points, respectively. All these three points satisfy the constraints discussed in the last section.

---

<sup>2</sup> Our choice of parameter space gives six heavy neutrinos ( $\nu_k$ ,  $k = 4, 5, \dots, 8, 9$ ) of which four are taken to be heavier than  $M_{Z'}$ . The lighter ones are nearly degenerate in mass, which we identify as  $N$  ( $\nu_4, \nu_5 \in N$ ) in our analysis.

	BP1	BP2	BP3
$M_{Z'} \text{ (GeV)}$	300	400	500
$M_N = \hat{M}_{N_{11}} \text{ (GeV)}$	120	150	200
$g_x$	0.149	0.191	0.246
$g'_x \times 10^3$	7.02	9.52	9.52
$\tan \theta' \times 10^4$	9.87	7.20	4.52
$\sigma(pp \rightarrow Z') \text{ (fb)}$	215.5	148.2	67.7
$\text{BR}(Z' \rightarrow NN)$	0.987	0.985	0.990
$\text{BR}(N \rightarrow \ell^\pm W^\mp(\nu Z))$	0.75 (0.25)	0.67 (0.29)	0.60 (0.29)

TABLE IV. Input parameters for the three benchmark points and the corresponding masses and mixing angles considered for our collider analysis (rounded off to the nearest digit). Note that we fix  $\tan \beta = 0.01$ ,  $Y_{\nu_{11}} = 0.06$ ,  $Y_{\nu_{22}} = Y_{\nu_{33}} = 0.2$ ,  $Y_{L_{11}} = 10^{-17}$ ,  $Y_{L_{22}} = 10^{-13}$ ,  $Y_{L_{33}} = 5.7 \times 10^{-13}$  and  $\hat{M}_{N_{22}} = \hat{M}_{N_{33}} = 1 \text{ TeV}$  for all benchmark points while  $\lambda_s \simeq 0.884$  (0.904) for BP1, BP2 (BP3) and  $v_s \simeq 1.01, 1.05, 1.02 \text{ TeV}$  for BP1, BP2, BP3, respectively.

Before discussing each specific analysis, we would like to mention the public packages that we have employed to perform the analysis. The model was implemented in **SARAH** [64] to get the **Universal Feynman Object** (UFO) [65] files. **SPheno** [66, 67] was used to generate the mass for the particle spectrum as well as the mixing parameters and mixing matrices connecting the gauge eigenstates to their mass eigenstates. The UFO model files were then used to calculate the scattering process with **Madgraph** and generate parton-level events with the **MadEvent** event generator using the package **MadGraph5@aMCNLO** (v2.6.7) [68, 69] at LHC with 14 TeV center-of-mass energy. These parton-level events were then showered with the help of **Pythia 8** [70]. Detector effects were simulated using fast detector simulation in **Delphes-3** [71] using the default ATLAS card. The final events were analysed using the analysis package **MadAnalysis5** [72] to present our results.

#### A. $4\ell + \cancel{E}_T$ final state

The  $4\ell$  final state is a relatively background free and clean event sample to study at the LHC. Some model dependent analysis has been carried out by experiments at the LHC to

look for such final states [73, 74]. We have checked that these analyses do not add any further constraints on our choice of the benchmark points. The four-lepton final state in our case occurs when both the  $W$  and  $Z$  bosons coming from each  $N$ , decay leptonically. In the case of  $N \rightarrow \ell W$  we expect MET from the neutrinos coming from the  $W$  decay while the  $N$  decays directly to neutrinos in the  $Z$  channel. Although the branching ratios of leptonic decay modes of  $W$  and  $Z$  is much smaller compared to their hadronic decay modes, higher charged lepton multiplicity in the final states are known to provide a cleaner signal with smaller SM background at a hadron collider. Thus the backgrounds for multi-lepton final states are manageable to negligible sizes at a hadron machine. This is one of the primary motivations behind the study of a  $4\ell$  final state at the LHC.

The major SM background for the  $4\ell + \cancel{E}_T$  final state comes from the following subprocesses [58]:

$$pp \rightarrow VZ, \quad pp \rightarrow t\bar{t}Z, \quad pp \rightarrow VVV \quad (V \equiv W^\pm, Z).$$

All SM backgrounds were generated using the same event generator as in the case of the signal. We then scale the background cross-section with their respective  $k$ -factors to make up for the NNLO corrections for  $ZZ$  and NLO corrections for  $t\bar{t}Z$  and  $VVV$  backgrounds. The  $k$ -factors are taken to be  $\simeq 1.72, 1.38, 2.01$  and  $2.27$  for  $ZZ$  [75],  $t\bar{t}Z$  [76],  $WZ$  [77] and  $VVV$  [78, 79], respectively.

For our analysis, we choose events which have exactly  $N_\ell = 4$  isolated charged leptons ( $\ell = e, \mu$ ) in the final state. As basic acceptance cuts, we demand that all reconstructed objects are isolated ( $\Delta R_{ab} > 0.4$ ). In addition,

- all charged leptons must have  $p_{T_\ell} > 10$  GeV and lie within the rapidity gap satisfying  $|\eta_\ell| < 2.5$ .
- We impose additional conditions to demand a hadronically quite environment by putting veto on events with light jets and  $b$  jets with  $p_{T_{b/j}} > 30$  GeV and  $|\eta_{b/j}| < 2.5$ . This helps in suppressing a significant part of the background coming from  $t\bar{t}(Z)$  production.
- We also demand a veto on any photon in the final state with  $p_T^\gamma > 10$  GeV and  $|\eta^\gamma| < 2.5$ .

Signal	Cross-section (fb)	SM Background	Cross-section (fb)
BP1	0.688	$ZZ$	9.088
BP2	0.476	$VVV$	0.111
BP3	0.204	$W^\pm Z$	0.081
		$t\bar{t} Z$	0.014

TABLE V. The cross-sections of signal and background for the final state  $pp \rightarrow 4\ell + \cancel{E}_T$  after the basic acceptance cuts and vetos.

We list the signal and background cross-sections after the basic acceptance cuts on the charged leptons and the veto on additional light jets,  $b$ -jets and photons in the final state in Table V. Note that with no requirement of MET in the final state, the dominant background comes from the  $pp \rightarrow ZZ$  subprocess.

To improve the signal to background ratio, one needs to exploit the kinematics of the signal events against that of the SM background. To achieve that, we must look at kinematic distributions of some relevant variables. In Fig. 6 and Fig. 7, we plot area normalized distributions for some of these important kinematic variables after detector simulation. In the left panel of Fig. 6, we note that the  $p_T$  distribution of the leading charged lepton peaks around 40–50 GeV for BP1, around 80–90 GeV for BP2 and around 100–120 GeV for BP3. These peaks are consistent with the mass difference between  $N$  and  $W$  ( $M_N - M_W$ ) for the three benchmark points (BPs) implying that the leading lepton comes from the primary decay of the heavy neutrino. We also note that with higher mass difference one expects to get the peak at a higher value of  $p_T$  for the signal. Thus a stronger  $p_T$  cut on the leading lepton would help remove the SM backgrounds with leading leptons on the softer side compared to the signal. However, the charged leptons in the SM background originate from the  $Z$  and  $W$  bosons and also show a peak around  $p_T \sim M_{Z/W}/2$  leading to a significant overlap with that of the signal events of BP1 and to some extent with that of the remaining two BPs too. The overlaps are significantly larger for the sub-leading leptons. Thus we choose a moderately smaller  $p_T > 20$  GeV requirement on the leading lepton, while all the remaining 3 leptons have  $p_T > 10$  GeV. The other important distributions correspond to the MET ( $\cancel{E}_T$ ) distribution and the invariant mass of the pair of oppositely charged same flavor (OSSF)



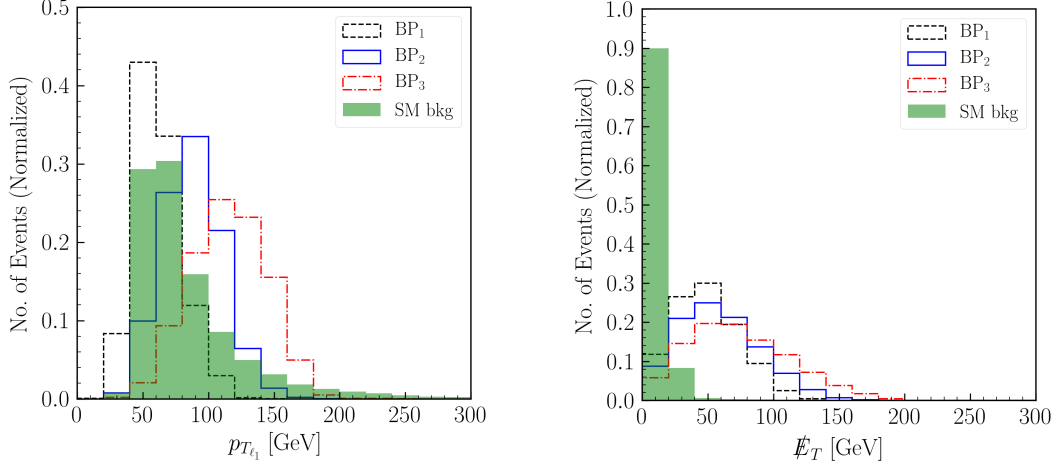


FIG. 6. Normalised distributions of  $p_{T_{\ell_1}}$  (left panel) and  $\cancel{E}_T$  (right panel) for  $4\ell + \cancel{E}_T$  final state at the 14 TeV LHC.

leptons *viz.*  $M_{e^+e^-}$  and  $M_{\mu^+\mu^-}$ . Note that for the  $ZZ$  background, the only source of MET would come from the imbalance in the visible  $p_T$  arising out of the mismeasurement of jet and lepton energies. Thus an MET cut of  $\cancel{E}_T > 15$  GeV helps us remove the  $ZZ$  background to a great extent without affecting the signal too much. The plot in the right panel of Fig. 6 supports this expectation. Note that as the particle spectrum is light and the corresponding decay products do not carry too much  $p_T$  we put an upper bound of 200 GeV on the  $p_T$  of the leading lepton and  $\cancel{E}_T$  which helps in suppressing some SM background. The effect of the aforementioned selection cuts are shown in Table VI.

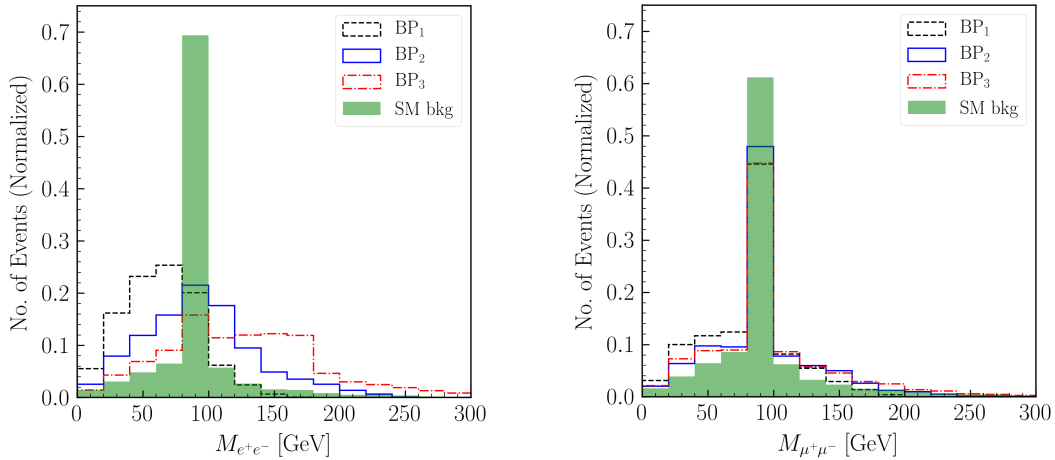


FIG. 7. Normalised distributions of  $M_{e^+e^-}$  (left panel) and  $M_{\mu^+\mu^-}$  (right panel) for  $4\ell + \cancel{E}_T$  final state at the 14 TeV LHC.

$\mathcal{L} = 100 \text{ fb}^{-1}$	SM-background				Signal		
Cuts	$ZZ$	$VVV$	$t\bar{t}Z$	$W^\pm Z$	BP1	BP2	BP3
$N_\mu \leq 2$	566.5	5.69	0.53	4.52	64.5	43.7	18.7
$(15 < \cancel{E}_T < 200) \text{ GeV}$	107.3	4.8	0.47	3.97	60.07	41.66	18.04
$(20 < p_{T_{\ell_1}} < 200) \text{ GeV}$	103.7	4.19	0.38	3.97	60.01	41.66	18.02
$M_{\mu^+\mu^-} < 80 \text{ GeV}$ or $M_{\mu^+\mu^-} > 95 \text{ GeV}$	35.35	2.74	0.25	3.6	56.17	38.5	16.6
Total Events after cuts	41.94				56.17	38.5	16.6
	Significance ( $\mathcal{S}$ )				7.38	5.67	2.42

TABLE VI. The cut-flow information on the  $pp \rightarrow 4\ell + \cancel{E}_T$  process for both the signal and background along with the significances for BP1, BP2, BP3 at 14 TeV LHC for  $100 \text{ fb}^{-1}$  integrated luminosity.

The invariant mass of  $e^+e^-$  and  $\mu^+\mu^-$  are shown in Fig. 7. We note that the signal events would not show a peak around the  $Z$  boson mass unless  $N$  decays via the  $(\nu Z)$  mode. For the backgrounds, the invariant mass of OSSF leptons peak at the  $Z$  boson mass. A large fraction of the signal events comes from  $N \rightarrow eW$  decay mode. Thus an invariant mass cut on the OSSF leptons of electron-type should be more useful in removing that background. However, as the  $p_{T_{e^\pm}}$  of the signal events are not very hard, we observe an overlap of the  $Z$  peak with the signal events in the  $M_{e^+e^-}$  distribution. So a cut of  $Z$  peak in the  $e^+e^-$  mode does not help a lot in improving the signal to background ratio. On the other hand, we expect that the fraction of events for the signal that contain at least a  $\mu^+\mu^-$  pair will be much smaller ( $\sim (28 - 31)\%$  for the 3 BPs) when compared to the full  $4\ell$  mode (as evident from the branching fractions of  $N$  and  $Z$ ). In contrast, the background is expected to be equally divided in the  $e$  and  $\mu$  modes. So although the normalized distribution in  $M_{\mu^+\mu^-}$  distribution shows a significant part of the signal in the mass bin of  $Z$  peak, we must realize that the distribution only corresponds to a very small fraction of the  $4\ell + \cancel{E}_T$  events after cuts. Therefore a cut to remove the  $Z$  peak in the  $\mu^+\mu^-$  distribution ( $80 < M_{\mu^+\mu^-} < 95 \text{ GeV}$ )<sup>3</sup> helps in suppressing a significant part of the SM background and improves the signal significance. To facilitate this we also demand that the four-lepton final state signal has at most a single pair of  $\mu^+\mu^-$ .

<sup>3</sup> The reason for an asymmetric cut around the  $Z$  mass is based on the fact that the invariant mass distribution from a resonant production always falls more rapidly beyond the parent particle mass.

The result of the analysis and the respective selection cuts are presented in Table VI for an integrated luminosity of  $\mathcal{L} = 100 \text{ fb}^{-1}$  at 14 TeV LHC.

We calculate the signal significance ( $\mathcal{S}$ ) by using the following formula.

$$\mathcal{S} = \sqrt{2 \left[ (S + B) \ln \left( \frac{S + B}{B} \right) - S \right]}, \quad (38)$$

where  $S$  and  $B$  are number of signal and background events, respectively. The signal significance for these three benchmark points are provided in the last column of Table VI. We can see that the signal for BP1 and BP2 have quite significant discovery potential as they correspond to a lighter  $Z'$  compared to BP3. The signal significance for a lighter  $Z'$  is high even with  $50 \text{ fb}^{-1}$  integrated luminosity, which may however be constrained by current LHC data. On the other hand such a constraint may be avoided by slight modification of the  $Z$ - $Z'$  mixing, as in the case of the di-lepton Drell-Yan channel. The important aspect of the above analysis however lies in the fact that signals for a light  $Z'$ , which does not talk to the SM particles directly may be absent in the di-lepton or di-jet modes but can be discovered in a more exotic  $4\ell + \cancel{E}_T$  channel.

### B. $3\ell + 2j + \cancel{E}_T$ final state

We now focus on the final state with a larger production rate as compared to the  $4\ell$  final state, viz. the  $3\ell + 2j + \cancel{E}_T$  signal at the LHC. However this channel has little advantage over the  $4\ell$  mode since the background events also become larger in this channel. The main SM background comes from the following subprocesses [58]:

$$pp \rightarrow VZ, \quad pp \rightarrow t\bar{t} + t\bar{t}Z, \quad pp \rightarrow VVV \quad (V \equiv W^\pm, Z).$$

As before, we include  $k$ -factors for the LO cross-section for the SM background to account for the NNLO correction for  $WZ$  and  $t\bar{t}$  and the NLO correction for  $VVV$  and  $t\bar{t}Z$  backgrounds. The  $k$ -factor is  $\simeq 1.6$  for  $t\bar{t}$  [80].

The object reconstruction to identify the final state particles is similar to what was done for the  $4\ell + \cancel{E}_T$  final state. The basic acceptance cuts considered for the  $3\ell + 2j + \cancel{E}_T$  signal are that all reconstructed objects are isolated ( $\Delta R_{ab} > 0.4$ ) and satisfy the following requirements.

Signal	Cross-section (fb)	SM Background	Cross-section (fb)
BP1	1.723	$ZZ$	1.528
BP2	1.526	$VVV$	0.266
BP3	0.717	$W^\pm Z$	37.23
		$t\bar{t} + t\bar{t} Z$	1.745

TABLE VII. The cross-sections of signal and background for the final state  $pp \rightarrow 3\ell + 2j + \cancel{E}_T$  after the basic acceptance cuts and vetos.

- We have exactly 3 charged leptons,  $N_\ell = 3$  ( $\ell = e, \mu$ ) in the final state, each with  $p_{T_\ell} > 10$  GeV and lying within the rapidity gap  $|\eta_\ell| < 2.5$ .
- We have exactly 2 light jets,  $N_j = 2$  in the final state, each with  $p_{T_j} > 30$  GeV and lying within the rapidity gap  $|\eta_j| < 2.5$ .
- We impose veto on events with a  $b$  jet having  $p_{T_b} > 30$  GeV and  $|\eta_b| < 2.5$ . This again helps in suppressing a significant part of the background coming from  $t\bar{t}(Z)$  production.
- We also demand a veto on any photon in the final state with  $p_T^\gamma > 10$  GeV and  $|\eta^\gamma| < 2.5$ .

We list the signal and background cross-sections after the basic acceptance cuts on the charged leptons, jets and a veto on any  $b$ -jet and photons in the final state in Table VII. We find that with the  $b$ -jet veto the  $t\bar{t}$  cross-section becomes quite small whereas the leading background comes from the  $WZ$ +jets final state where both the gauge bosons decay leptonically to give 3 charged leptons in the final state. For the signal, we again expect the dominant contribution to come from the  $N \rightarrow eW$  decay mode, where one of the  $W$  decays hadronically to 2 jets.

As we note that the signal is rich in  $e^\pm$  and the  $\mu$  multiplicity peaks at one, it again seems beneficial to put a constraint on  $N_\mu \leq 1$  which should not affect the signal too much while suppressing the SM background. This can be seen from the cut-flow numbers presented in Table VIII. We now look at the distributions of some of the important variables for this final state which are shown in Figs. 8 and 9. In Fig. 8 we plot the  $p_T$  distribution of the leading

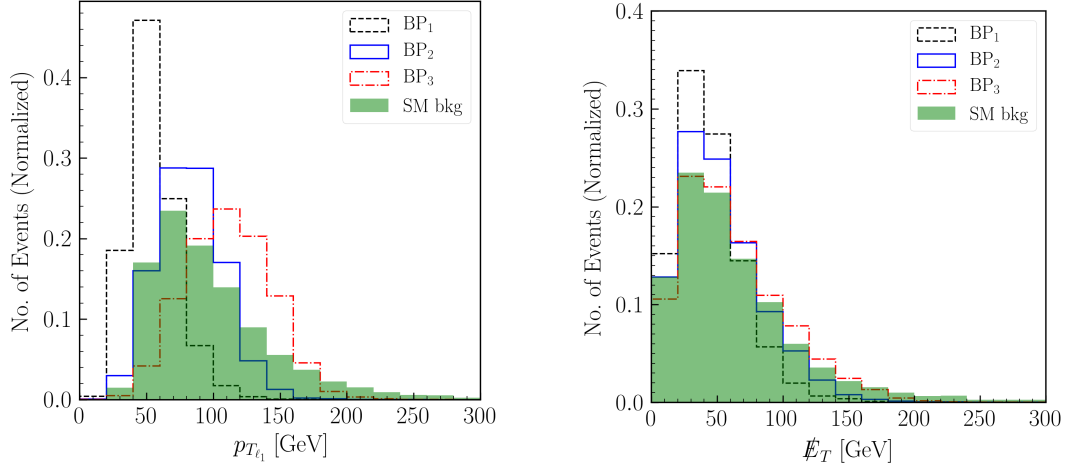


FIG. 8. Normalised distributions of  $p_{T_{\ell_1}}$  (left panel) and  $\cancel{E}_T$  (right panel) for  $3\ell + 2j + \cancel{E}_T$  final state at the 14 TeV LHC.

lepton as well as the  $\cancel{E}_T$  distribution. The lepton  $p_T$  shows a similar behaviour to the case of  $4\ell$  final state and therefore we stick to a similar selection cut on the leading lepton to have  $p_T > 20$  GeV. The  $\cancel{E}_T$  distribution is markedly different due to the contributions from other background processes dominating over the ones that contributed to the  $4\ell + \cancel{E}_T$  case. However, we still note that the  $\cancel{E}_T > 15$  GeV cut will suppress the  $ZZ$  background as seen in Table VIII. As in the case of  $4\ell + \cancel{E}_T$  we again put an upper bound of 200 GeV on the  $p_T$  of the leading lepton and  $\cancel{E}_T$  to suppress the SM background which has a longer tail in the distributions extending beyond 200 GeV.

In Fig. 9 we plot the  $p_T$  of the leading jet and the invariant mass distribution in  $e^+e^-$ . As the jets for the signal are not expected to be hard, we put an upper bound on them as  $p_{T_{j_1}} < 200$  GeV. The dominant suppression in the background comes from the invariant mass cut where we remove the  $Z$  peak. As we expect the electron or positron ( $e$ ) to come from the decay of  $N$  for the signal, we expect no  $Z$  peak in the signal. Thus the invariant mass cut along with the constraint on  $\mu$  multiplicity proves to be the most important condition that improve the  $S/B$  for the  $3\ell + 2j + \cancel{E}_T$  final state.

The result of the analysis and the respective selection cuts are presented in Table VIII for an integrated luminosity of  $\mathcal{L} = 100 \text{ fb}^{-1}$  at 14 TeV LHC. We can see that, as in the case of  $4\ell + \cancel{E}_T$ , the signal for BP1 and BP2 again has quite large significance, albeit slightly smaller for the same integrated luminosity. The above analysis however shows that both the

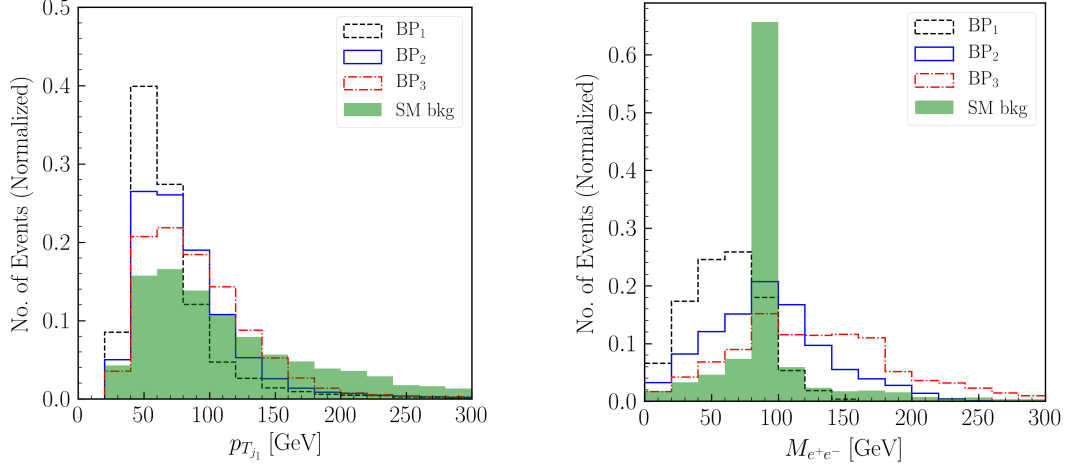


FIG. 9. Normalised distributions of  $p_{T_{j1}}$  (left panel) and  $M_{e^+e^-}$  (right panel) for  $3\ell + 2j + \cancel{E}_T$  final state at the 14 TeV LHC.

$\mathcal{L} = 100 \text{ fb}^{-1}$		SM-background				Signal		
Cuts		$W^\pm Z$	$t\bar{t} + t\bar{t}Z$	$ZZ$	$VVV$	BP1	BP2	BP3
$N_\mu \leq 1$		2246.0	147.2	86.5	26.0	170.4	150.6	70.7
$(15 < \cancel{E}_T < 200) \text{ GeV}$		2022.0	146.2	39.0	22.1	155.0	139.4	66.1
$p_T^{j1} < 200 \text{ GeV}$		1686.0	119.3	35.7	18.8	152.1	135.8	64.0
$(20 < p_{T_{\ell_1}} < 200) \text{ GeV}$		1608.0	118.7	34.6	17.2	151.4	135.7	63.7
$M_{e^+e^-} < 85 \text{ GeV or } M_{e^+e^-} > 95 \text{ GeV}$		228.0	97.3	4.9	2.2	124.9	96.0	49.0
Total Events after cuts		86.3				124.9	96.0	49.0
		Significance ( $\mathcal{S}$ )				6.48	5.04	2.63

TABLE VIII. The cut-flow information on the  $pp \rightarrow 3\ell + 2j + \cancel{E}_T$  process for both the signal and background along with the significances for BP1, BP2, BP3 at 14 TeV LHC for  $100 \text{ fb}^{-1}$  integrated luminosity.

$3\ell$  and  $4\ell$  final states show a promising discovery channel for light  $Z'$  which does couple to the SM particles directly, with the higher lepton multiplicity case doing slightly better. The analysis can be extended to include heavier  $Z'$  as well and consider the other final states available for the  $Z'$ , which would be similar to the more traditional  $Z'$  searches such as the  $U(1)_{B-L}$  models for example [57, 59].

## V. SUMMARY AND OUTLOOK

We consider a neutrinophilic model as an extension of the SM by introducing a  $U(1)$  group which couples directly to only heavy neutral fermions, singlet under the SM. The neutral fermion charged under the new group couples to the SM matter fields through Yukawa interactions via a neutrinophilic scalar doublet. The neutrinos in the model get their mass from a standard inverse-seesaw mechanism while an added scalar sector is responsible for the breaking of the gauged  $U(1)$  leading to light neutral gauge boson ( $Z'$ ). We study the phenomenology of having such a light  $Z'$  in the context of neutrinophilic interactions as well as the role of allowing kinetic mixing between the new  $U(1)$  group with the SM hypercharge group. We show that current experimental searches allow for a very light  $Z'$  if it does not couple to SM fields directly and highlight the search strategies at the LHC.

To highlight the features of the model, we calculate the mass and mixing of the scalar, gauge and matter fields after symmetry breaking and look at the experimental constraints on the model parameters. We find that once the scalar sector is set to agree with the Higgs searches, by choosing the lightest CP even scalar to be the 125 GeV SM Higgs boson, the  $Z'$  phenomenology is only dependent on the  $Z$ - $Z'$  mixing and its coupling to the heavy neutral fermions. Following an examination of the allowed region for the mixing angle and the  $U(1)_X$  gauge coupling we determine two regions of parameter space depending upon the value of  $\tan\beta$ , the ratio of the doublet VEVs. For  $\tan\beta > 1$  we find an upper bound on the ratio  $v_2/v_1 < 3$  from the perturbativity requirement on the fermion-fermion scalar couplings. We also observe that  $g_x$  and  $g'_x$  are of the same order when  $\tan\beta > 1$  which gives us a  $Z'$  phenomenology driven by the  $Z$ - $Z'$  mixing angle  $\sin\theta'$  with the dominant decay to SM fermion pair. A more interesting scenario emerges for  $\tan\beta < 1$  where the  $g'_x$  and  $g_x$  are no longer required to be of the same order anymore. We find that the  $Z'$  signatures are now dependent on the interplay of the  $Z$ - $Z'$  mixing as well as the  $U(1)_X$  gauge coupling  $g_x$  which is allowed to be large. Thus the  $Z'$  can now decay dominantly to a pair of heavy neutrinos while the  $Z'$  is produced through the  $Z$ - $Z'$  mixing parameter driven by  $g'_x$ . We analyse the signal for such a scenario at the LHC with  $\sqrt{s} = 14$  TeV in the  $4\ell + \cancel{E}_T$  and  $3\ell + 2j + \cancel{E}_T$  channels for a  $Z'$  lying in the mass range 200–500 GeV. We find that although the di-lepton Drell-Yan channel is much suppressed here, the discovery prospects of observing a neutrinophilic  $Z'$  is significantly high in the above channels. We show the significance

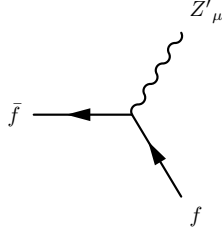
of the signal using an integrated luminosity of  $100 \text{ fb}^{-1}$  for three benchmark points. We conclude that multi-lepton final states could be crucial in discovering such a neutrinophilic gauge boson lying in the mass range of 200–500 GeV with even a very tiny gauge-kinetic mixing of the order  $\mathcal{O}(10^{-3})$ .

We must point out here that other interesting signatures of the  $Z'$  in such a model is being left for future work, which include flavor violating decays of the  $Z'$ , a more detailed analysis of the scalar sector with the  $Z'$  and implications of a very light  $Z'$  and a singlet scalar [81].

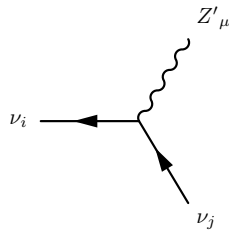
## VI. APPENDIX

### A. Coupling of $Z'$ gauge boson with fermions

We list below the coupling of the  $Z'$  gauge boson with the fermions in the model. We define  $s_W \equiv \sin \theta_W$  and  $c_W \equiv \cos \theta_W$  where  $\theta_W$  is the Weinberg angle while  $s_{\theta'} \equiv \sin \theta'$  and  $c_{\theta'} \equiv \cos \theta'$  where  $\theta'$  is the  $Z$ - $Z'$  mixing angle. In addition,  $T_3$  and  $Q_f$  represent the isospin and electric charge of the fermions, respectively, while  $P_{L/R} = \frac{1 \mp \gamma_5}{2}$  are the projection operators.



$$i \left( \frac{e s_{\theta'}}{s_W c_W} (T^3 - Q_f s_W^2) + g'_x c_{\theta'} (T^3 - Q_f) \right) \gamma^\mu P_L - i \left( \frac{e s_{\theta'}}{s_W c_W} Q_f s_W^2 + g'_x c_{\theta'} Q_f \right) \gamma^\mu P_R$$





$$\frac{i}{2} \left( \left( \frac{e s_{\theta'}}{2 s_W c_W} + \frac{g'_x}{2} c_{\theta'} \right) \sum_{k=1}^3 \mathcal{N}_{ik} \mathcal{N}_{jk}^* - g_x c_{\theta'} \sum_{k=4}^9 \mathcal{N}_{ik} \mathcal{N}_{jk}^* \right) \gamma^\mu,$$

where  $\mathcal{N}$  is the neutrino mixing matrix as defined in Eq. (36). We note that  $\nu_i$  for  $i = 1, 2, 3$  are identified as the light neutrinos and rest are heavy neutrinos. These neutrinos are Majorana fermions written in 4-component notation.

## VII. ACKNOWLEDGEMENT

The authors would like to acknowledge support from the Department of Atomic Energy, Government of India, for the Regional Centre for Accelerator-based Particle Physics (RECAPP). WA acknowledges support from the XII Plan Neutrino Project of the Department of Atomic Energy.

- 
- [1] G. Aad *et al.* (ATLAS), *Phys. Lett. B* **716**, 1 (2012), [arXiv:1207.7214 \[hep-ex\]](#).
  - [2] S. Chatrchyan *et al.* (CMS), *Phys. Lett. B* **716**, 30 (2012), [arXiv:1207.7235 \[hep-ex\]](#).
  - [3] Y. Fukuda *et al.* (Super-Kamiokande), *Phys. Rev. Lett.* **81**, 1562 (1998), [arXiv:hep-ex/9807003](#).
  - [4] A. Aguilar-Arevalo *et al.* (LSND), *Phys. Rev. D* **64**, 112007 (2001), [arXiv:hep-ex/0104049](#).
  - [5] M. H. Ahn *et al.* (K2K), *Phys. Rev. Lett.* **90**, 041801 (2003), [arXiv:hep-ex/0212007](#).
  - [6] K. Abe *et al.* (T2K), *Phys. Rev. Lett.* **107**, 041801 (2011), [arXiv:1106.2822 \[hep-ex\]](#).
  - [7] F. P. An *et al.* (Daya Bay), *Phys. Rev. Lett.* **112**, 061801 (2014), [arXiv:1310.6732 \[hep-ex\]](#).
  - [8] P. Minkowski, *Phys. Lett. B* **67**, 421 (1977).
  - [9] R. N. Mohapatra and G. Senjanovic, *Phys. Rev. Lett.* **44**, 912 (1980).
  - [10] M. Gell-Mann, P. Ramond, and R. Slansky, *Conf. Proc. C* **790927**, 315 (1979), [arXiv:1306.4669 \[hep-th\]](#).
  - [11] T. Yanagida, *Conf. Proc. C* **7902131**, 95 (1979).
  - [12] S. L. Glashow, in *Quarks and Leptons*, edited by M. Lévy, J.-L. Basdevant, D. Speiser, J. Weyers, R. Gastmans, and M. Jacob (Springer US, Boston, MA, 1980) pp. 687–713.
  - [13] M. C. Gonzalez-Garcia and M. Maltoni, *Phys. Rept.* **460**, 1 (2008), [arXiv:0704.1800 \[hep-ph\]](#).

- [14] E. Ma, *Phys. Rev. Lett.* **86**, 2502 (2001), [arXiv:hep-ph/0011121](#).
- [15] S. Gabriel and S. Nandi, *Phys. Lett. B* **655**, 141 (2007), [arXiv:hep-ph/0610253](#).
- [16] S. M. Davidson and H. E. Logan, *Phys. Rev. D* **80**, 095008 (2009), [arXiv:0906.3335 \[hep-ph\]](#).
- [17] S. Gabriel, B. Mukhopadhyaya, S. Nandi, and S. K. Rai, *Phys. Lett. B* **669**, 180 (2008), [arXiv:0804.1112 \[hep-ph\]](#).
- [18] S. M. Davidson and H. E. Logan, *Phys. Rev. D* **82**, 115031 (2010), [arXiv:1009.4413 \[hep-ph\]](#).
- [19] N. Haba and K. Tsumura, *JHEP* **06**, 068 (2011), [arXiv:1105.1409 \[hep-ph\]](#).
- [20] W. Chao and M. J. Ramsey-Musolf, *Phys. Rev. D* **89**, 033007 (2014), [arXiv:1212.5709 \[hep-ph\]](#).
- [21] U. Maitra, B. Mukhopadhyaya, S. Nandi, S. K. Rai, and A. Shivaji, *Phys. Rev. D* **89**, 055024 (2014), [arXiv:1401.1775 \[hep-ph\]](#).
- [22] Huitu, Katri and Karkkainen, Timo J. and Mondal, Subhadeep and Rai, Santosh Kumar, *Phys. Rev. D* **97**, 035026 (2018), [arXiv:1712.00338 \[hep-ph\]](#).
- [23] B. N. Grossmann, B. McElrath, S. Nandi, and S. K. Rai, *Phys. Rev. D* **82**, 055021 (2010), [arXiv:1006.5019 \[hep-ph\]](#).
- [24] K. Das and S. K. Rai, *Phys. Rev. D* **93**, 095007 (2016), [arXiv:1512.07789 \[hep-ph\]](#).
- [25] P. Langacker, *Rev. Mod. Phys.* **81**, 1199 (2009), [arXiv:0801.1345 \[hep-ph\]](#).
- [26] E. Accomando, D. Becciolini, A. Belyaev, S. De Curtis, D. Dominici, S. F. King, S. Moretti, and C. Shepherd-Themistocleous, *PoS DIS2013*, 125 (2013).
- [27] M. Aaboud *et al.* (ATLAS), *JHEP* **10**, 182 (2017), [arXiv:1707.02424 \[hep-ex\]](#).
- [28] A. M. Sirunyan *et al.* (CMS), *Phys. Rev. Lett.* **124**, 131802 (2020), [arXiv:1912.04776 \[hep-ex\]](#).
- [29] P. H. Chankowski, S. Pokorski, and J. Wagner, *Eur. Phys. J. C* **47**, 187 (2006), [arXiv:hep-ph/0601097](#).
- [30] R. N. Mohapatra and J. W. F. Valle, *Phys. Rev. D* **34**, 1642 (1986).
- [31] S. Nandi and U. Sarkar, *Phys. Rev. Lett.* **56**, 564 (1986).
- [32] R. N. Mohapatra, *Phys. Rev. Lett.* **56**, 561 (1986).
- [33] G. 't Hooft, *NATO Sci. Ser. B* **59**, 135 (1980).
- [34] A. Das and N. Okada, *Phys. Rev. D* **88**, 113001 (2013), [arXiv:1207.3734 \[hep-ph\]](#).
- [35] P. S. B. Dev, A. Pilaftsis, and U.-k. Yang, *Phys. Rev. Lett.* **112**, 081801 (2014), [arXiv:1308.2209 \[hep-ph\]](#).

- [36] A. Das, P. S. Bhupal Dev, and N. Okada, *Phys. Lett. B* **735**, 364 (2014), [arXiv:1405.0177 \[hep-ph\]](#).
- [37] F. F. Deppisch, P. S. Bhupal Dev, and A. Pilaftsis, *New J. Phys.* **17**, 075019 (2015), [arXiv:1502.06541 \[hep-ph\]](#).
- [38] S. Mondal and S. K. Rai, *Phys. Rev. D* **94**, 033008 (2016), [arXiv:1605.04508 \[hep-ph\]](#).
- [39] P. A. Zyla *et al.* (Particle Data Group), *PTEP* **2020**, 083C01 (2020).
- [40] P. S. B. Dev and R. N. Mohapatra, *Phys. Rev. D* **81**, 013001 (2010), [arXiv:0910.3924 \[hep-ph\]](#).
- [41] W. Abdallah, A. Awad, S. Khalil, and H. Okada, *Eur. Phys. J. C* **72**, 2108 (2012), [arXiv:1105.1047 \[hep-ph\]](#).
- [42] S. Antusch, C. Biggio, E. Fernandez-Martinez, M. B. Gavela, and J. Lopez-Pavon, *JHEP* **10**, 084 (2006), [arXiv:hep-ph/0607020](#).
- [43] M. Malinsky, T. Ohlsson, Z.-z. Xing, and H. Zhang, *Phys. Lett. B* **679**, 242 (2009), [arXiv:0905.2889 \[hep-ph\]](#).
- [44] A. Ibarra, E. Molinaro, and S. T. Petcov, *Phys. Rev. D* **84**, 013005 (2011), [arXiv:1103.6217 \[hep-ph\]](#).
- [45] P. F. de Salas, D. V. Forero, C. A. Ternes, M. Tortola, and J. W. F. Valle, *Phys. Lett. B* **782**, 633 (2018), [arXiv:1708.01186 \[hep-ph\]](#).
- [46] M. Aaboud *et al.* (ATLAS), *Phys. Rev. D* **98**, 052005 (2018), [arXiv:1802.04146 \[hep-ex\]](#).
- [47] A. M. Sirunyan *et al.* (CMS), *JHEP* **11**, 185 (2018), [arXiv:1804.02716 \[hep-ex\]](#).
- [48] A. M. Sirunyan *et al.* (CMS), *Phys. Lett. B* **779**, 283 (2018), [arXiv:1708.00373 \[hep-ex\]](#).
- [49] M. Aaboud *et al.* (ATLAS), *Phys. Rev. D* **98**, 052003 (2018), [arXiv:1807.08639 \[hep-ex\]](#).
- [50] (2018).
- [51] A. M. Sirunyan *et al.* (CMS), *Phys. Lett. B* **791**, 96 (2019), [arXiv:1806.05246 \[hep-ex\]](#).
- [52] (2019).
- [53] G. Aad *et al.* (ATLAS), *Phys. Lett. B* **798**, 134949 (2019), [arXiv:1903.10052 \[hep-ex\]](#).
- [54] P. Bechtle, S. Heinemeyer, O. Stål, T. Stefaniak, and G. Weiglein, *Eur. Phys. J. C* **74**, 2711 (2014), [arXiv:1305.1933 \[hep-ph\]](#).
- [55] P. Bechtle, O. Brein, S. Heinemeyer, G. Weiglein, and K. E. Williams, *Comput. Phys. Commun.* **181**, 138 (2010), [arXiv:0811.4169 \[hep-ph\]](#).
- [56] P. Bechtle, O. Brein, S. Heinemeyer, G. Weiglein, and K. E. Williams, *Comput. Phys. Commun.* **182**, 2605 (2011), [arXiv:1102.1898 \[hep-ph\]](#).

- [57] K. Huitu, S. Khalil, H. Okada, and S. K. Rai, *Phys. Rev. Lett.* **101**, 181802 (2008), [arXiv:0803.2799 \[hep-ph\]](#).
- [58] F. del Aguila and J. A. Aguilar-Saavedra, *Nucl. Phys. B* **813**, 22 (2009), [arXiv:0808.2468 \[hep-ph\]](#).
- [59] L. Basso, A. Belyaev, S. Moretti, and C. H. Shepherd-Themistocleous, *Phys. Rev. D* **80**, 055030 (2009), [arXiv:0812.4313 \[hep-ph\]](#).
- [60] P. Fileviez Perez, T. Han, and T. Li, *Phys. Rev. D* **80**, 073015 (2009), [arXiv:0907.4186 \[hep-ph\]](#).
- [61] A. Atre, T. Han, S. Pascoli, and B. Zhang, *JHEP* **05**, 030 (2009), [arXiv:0901.3589 \[hep-ph\]](#).
- [62] E. Accomando, C. Coriano, L. Delle Rose, J. Fiaschi, C. Marzo, and S. Moretti, *JHEP* **07**, 086 (2016), [arXiv:1605.02910 \[hep-ph\]](#).
- [63] P. Cox, C. Han, and T. T. Yanagida, *JHEP* **01**, 037 (2018), [arXiv:1707.04532 \[hep-ph\]](#).
- [64] F. Staub, *Comput. Phys. Commun.* **185**, 1773 (2014), [arXiv:1309.7223 \[hep-ph\]](#).
- [65] C. Degrande, C. Duhr, B. Fuks, D. Grellscheid, O. Mattelaer, and T. Reiter, *Comput. Phys. Commun.* **183**, 1201 (2012), [arXiv:1108.2040 \[hep-ph\]](#).
- [66] W. Porod, *Comput. Phys. Commun.* **153**, 275 (2003), [arXiv:hep-ph/0301101](#).
- [67] W. Porod and F. Staub, *Comput. Phys. Commun.* **183**, 2458 (2012), [arXiv:1104.1573 \[hep-ph\]](#).
- [68] J. Alwall, M. Herquet, F. Maltoni, O. Mattelaer, and T. Stelzer, *JHEP* **06**, 128 (2011), [arXiv:1106.0522 \[hep-ph\]](#).
- [69] J. Alwall, R. Frederix, S. Frixione, V. Hirschi, F. Maltoni, O. Mattelaer, H. S. Shao, T. Stelzer, P. Torrielli, and M. Zaro, *JHEP* **07**, 079 (2014), [arXiv:1405.0301 \[hep-ph\]](#).
- [70] T. Sjöstrand, S. Ask, J. R. Christiansen, R. Corke, N. Desai, P. Ilten, S. Mrenna, S. Prestel, C. O. Rasmussen, and P. Z. Skands, *Comput. Phys. Commun.* **191**, 159 (2015), [arXiv:1410.3012 \[hep-ph\]](#).
- [71] J. de Favereau, C. Delaere, P. Demin, A. Giammanco, V. Lemaître, A. Mertens, and M. Selvaggi (DELPHES 3), *JHEP* **02**, 057 (2014), [arXiv:1307.6346 \[hep-ex\]](#).
- [72] E. Conte, B. Fuks, and G. Serret, *Comput. Phys. Commun.* **184**, 222 (2013), [arXiv:1206.1599 \[hep-ph\]](#).
- [73] M. Aaboud *et al.* (ATLAS), *Phys. Rev. D* **98**, 032009 (2018), [arXiv:1804.03602 \[hep-ex\]](#).
- [74] G. Aad *et al.* (ATLAS), (2021), [arXiv:2101.11961 \[hep-ex\]](#).

- [75] F. Cascioli, T. Gehrmann, M. Grazzini, S. Kallweit, P. Maierhöfer, A. von Manteuffel, S. Pozzorini, D. Rathlev, L. Tancredi, and E. Weihs, *Phys. Lett. B* **735**, 311 (2014), [arXiv:1405.2219 \[hep-ph\]](#).
- [76] A. Kardos, Z. Trocsanyi, and C. Papadopoulos, *Phys. Rev. D* **85**, 054015 (2012), [arXiv:1111.0610 \[hep-ph\]](#).
- [77] M. Grazzini, S. Kallweit, D. Rathlev, and M. Wiesemann, *Phys. Lett. B* **761**, 179 (2016), [arXiv:1604.08576 \[hep-ph\]](#).
- [78] H. Wang, R.-Y. Zhang, W.-G. Ma, L. Guo, X.-Z. Li, and S.-M. Wang, *J. Phys. G* **43**, 115001 (2016), [arXiv:1610.05876 \[hep-ph\]](#).
- [79] Y.-B. Shen, R.-Y. Zhang, W.-G. Ma, X.-Z. Li, and L. Guo, *Phys. Rev. D* **95**, 073005 (2017), [arXiv:1605.00554 \[hep-ph\]](#).
- [80] M. Czakon, P. Fiedler, and A. Mitov, *Phys. Rev. Lett.* **110**, 252004 (2013), [arXiv:1303.6254 \[hep-ph\]](#).
- [81] W. Abdallah, A. K. Barik, S. K. Rai, and T. Samui, Work in Progress (2021).